BRNO UNIVERSITY OF TECHNOLOGY

Faculty of Mechanical Engineering

MASTER'S THESIS

Brno, 2024 Bc. Giorgi Tabukashvili

BRNO UNIVERSITY OF TECHNOLOGY

VYSOKÉ UČENÍ TECHNICKÉ V BRNĚ

FACULTY OF MECHANICAL ENGINEERING

FAKULTA STROJNÍHO INŽENÝRSTVÍ

INSTITUTE OF AUTOMOTIVE ENGINEERING

ÚSTAV AUTOMOBILNÍHO A DOPRAVNÍHO INŽENÝRSTVÍ

ANALYSIS OF SURFACE DEFORMATIONS OF THE TURBOCHARGER ROTOR AT THE LOCATION OF THE RADIAL BEARING

ANALÝZA DEFORMACÍ POVRCHU ROTORU TURBODMYCHADLA V MÍSTĚ RADIÁLNÍHO LOŽISKA

MASTER'S THESIS

DIPLOMOVÁ PRÁCE

AUTHOR — Bc. Giorgi Tabukashvili

AUTOR PRÁCE

SUPERVISOR — prof. Ing. Pavel Novotný, Ph.D.

VEDOUCÍ PRÁCE

BRNO 2024

Giorgi Tabukashvili

ANALYSIS OF SURFACE DEFORMATIONS OF THE TURBOCHARGER ROTOR AT THE LOCATION OF THE RADIAL BEARING

BRNO UNIVERSITY OF TECHNOLOGY
FACULTY OF MECHANICAL ENGINEERING

Assignment Master's Thesis

Institute:	Institute of Automotive Engineering
Student:	**Bc. Giorgi Tabukashvili**
Degree program:	Mechanical Engineering
Branch:	no specialization
Supervisor:	**prof. Ing. Pavel Novotný, Ph.D.**
Academic year:	2024/25

As provided for by the Act No. 111/98 Coll. on higher education institutions and the BUT Study and Examination Regulations, the director of the Institute hereby assigns the following topic of Master's Thesis:

Analysis of surface deformations of the turbocharger rotor at the location of the radial bearing

Brief Description:

The rotors of turbochargers are subjected to high thermal–mechanical loads. The work focuses on the turbocharger of a ten–cylinder stationary internal combustion engine with an output of 1.6 MW. Significant rotor deformations occur at the journal bearing locations under turbocharger operation, mainly due to uneven temperature distribution. These deformations result in a change in the shape of the bearing lubrication gap. The work deals with the evaluation of the deformation at the journal bearing location in steady state operation under simultaneous application of thermal load and mechanical load due to preload and rotation.

Master's Thesis goals:

Review of turbocharger rotor deformations under thermo–mechanical loading.
Analysis of the rotor temperature field at the journal bearing location under steady state operation. Analysis of rotor surface deformation at the journal bearing location under steady state operation.

Recommended bibliography:

BENINI, Ernesto. Advances in Gas Turbine Technology. 2011. ISBN 978-953-307-611-9.

MILLER, Jay. Turbo: Real World High-Performance Turbocharger Systems. Michigan, USA: CarTech, 2008. ISBN 978-1932494297.

STACHOWIAK, G. W. a A. W. BATCHELOR. Engineering Tribology. 3. vyd. Boston: Elsevier Butterworth-Heinemann, 2005. ISBN 0-7506-7836-4.

NGUYEN-SCHÄFER, H. Rotordynamics of Automotive Turbochargers. Second Edition. Ludwigsburg, Germany: Springer, 2015. ISBN 978-3-319-17643-7.

Deadline for submission Master's Thesis is given by the Schedule of the Academic year 2024/25

In Brno,

L. S.

prof. Ing. Josef Štětina, Ph.D.
Director of the Institute

doc. Ing. Jiří Hlinka, Ph.D.
FME dean

Abstract

The rotors of turbochargers are subjected to high thermal–mechanical loads. The work focuses on the turbocharger of a ten–cylinder stationary internal combustion engine with an output of 1.6 MW. Significant rotor deformations occur at the journal bearing locations under turbocharger operation, mainly due to uneven temperature distribution. These deformations result in a change in the shape of the bearing lubrication gap. The work deals with the evaluation of the deformation at the journal bearing location in steady state operation under simultaneous application of thermal load and mechanical load due to preload and rotation. More precisely the goal is to Review of turbocharger rotor deformations under thermo–mechanical loading. By analyzing the rotor temperature field at the journal bearing location under steady state operation. And analyzing the rotor surface deformation at the journal bearing location under steady state operation.

Key words:

Heat transfer, turbocharger, FEM, Journal bearing.

BIBLIOGRAPHIC CITATION

Printed work citation:

TABUKASHVILI, Giorgi. Analysis of surface deformations of the turbocharger rotor at the location of the radial bearing. Brno, 2025. Available also at: https://www.vut.cz/studenti/zav-prace/detail/162441. Master's Thesis. Vysoké učení technické v Brně, Fakulta strojního inženýrství, Institute of Automotive Engineering. Supervisor Pavel Novotný.

Electronic source citation:

TABUKASHVILI, Giorgi. Analysis of surface deformations of the turbocharger rotor at the location of the radial bearing [online]. Brno, 2025 [cit. 2024-08-29]. Available from: https://www.vut.cz/studenti/zav-prace/detail/162441. Master's Thesis. Vysoké učení technické v Brně, Fakulta strojního inženýrství, Institute of Automotive Engineering. Supervisor Pavel Novotný.

DECLARATION OF AUTHENTICITY

I so certify that I did not receive any outside help when writing my master's thesis, " Analysis of surface deformations of the turbocharger rotor at the location of the radial bearing." I have properly cited every paragraph in the thesis that comes from outside sources, including any graphics, tables, and the like. I did not utilise any other sources but those included in the bibliography. No other degree program has ever received this thesis in its current or comparable form.

17.05.2025

Date

Giorgi Tabukashvili

ACKNOWLEDGEMENT

To my supervisor, prof. Ing. Pavel Novotný, Ph.D., I would like to express my gratitude for his patient instruction, support, and counsel.

Table of Contents

Analysis of surface deformations of the turbocharger rotor at the location of the radial bearing

Abstract

The rotors of turbochargers are subjected to high thermal–mechanical loads. The work focuses on the turbocharger of a ten–cylinder stationary internal combustion engine with an output of 1.6 MW. Significant rotor deformations occur at the journal bearing locations under turbocharger operation, mainly due to uneven temperature distribution. These deformations result in a change in the shape of the bearing lubrication gap. The work deals with the evaluation of the deformation at the journal bearing location in steady state operation under simultaneous application of thermal load and mechanical load due to preload and rotation. More precisely the goal is to Review of turbocharger rotor deformations under thermo–mechanical loading. By analyzing the rotor temperature field at the journal bearing location under steady state operation. And analyzing the rotor surface deformation at the journal bearing location under steady state operation.

1. Introduction

The most critical component of internal combustion engines, and the technology that enhances their performance, is the turbocharger. A comprehensive understanding of the concept of turbochargers necessitates a foundation in the principles of engine functioning. The primary function of an engine as a mechanical system is to transform thermal energy into mechanical energy. The most prevalent 4-stroke internal combustion (IC) engine accomplishes this transformation during its operational cycle, which necessitates two revolutions of the crankshaft at 720 degrees Fahrenheit. This process occurs during combustion, when the system performs the work [1]. It is noteworthy that leading engine manufacturers have acknowledged that the potential for enhancing airflow through short block engine design has essentially reached its limits. The design of the cylinder head and intake manifold, which contain the trade secrets for professional stock competitors to increase airflow, is of particular interest. This is due to the inherent limitations of naturally aspirated engines, which lack forced air induction systems. The overarching objective of engine design is to maximize power output while operating within a series of constraints. It is imperative that the engine receive a sufficient supply of fuel; this is not a significant concern. However, ensuring adequate air intake poses a substantial challenge. Turbos are a viable solution to this problem, but only to the extent that they can withstand the structural-thermal loads that occur during operation. Since engine power is only produced by combustion of fuel, and the more fuel burned, the greater the power gets, fuel must productively burn in an engine cylinder with enough air present to do it, but to have sufficiently enough air, we need to have a pressure difference between the atmosphere and the engine cylinder [1]. At sea level, atmospheric pressure is Patm = 0.10135 (MPa). This indicates that an engine's capacity to breathe is restricted by the suction, or vacuum, produced by the piston's intake stroke when fed by a pressure that is at most 0.10342 (MPa). Therefore, this value indicates that despite the best, most efficient design of the engine, there will be the maximum difference of approximately 0.10342 (MPa) absolute pressure between the intake valve and the atmosphere. This is where the turbocharger comes in. Basically, a turbocharger is a mechanical system whose purpose is to drive more air into the engine cylinders since the air is driven by the pressure created by the compressor. In the engine, there will be much more air than there was with only the help of a vacuum. Now fuel supply can be increased, and thus more power will be developed by the engine. A turbocharger mainly consists of three parts: the turbine, the compressor, and the bearing system, which connects these two together. Each of these parts has different developer specialists, but the parts must be dependent on each other in order to function properly [1]. The turbine is the receiver of the energy from the engine, which is basically the form of heat and pressure [1]. The turbine consists of two main components: the turbine wheel and the turbine housing. During high-pressure exhaust gas travel in between the turbine blades, it expands due to the shape of the blades and turbine housing. This exhaust gas expansion is the main source

that causes the turbine to come in motion. The turbine is a component that converts energy in the form of heat and pressure into mechanical energy, presented as a rotation of the turbine wheel. The compressor is a turbocharger's component that has two purposes: first, to raise the density of the fresh air by compressing it between its blades, and since the engine's cylinders have a fixed volumetric capacity, it is crucial to have it efficiently full. Therefore, the second job of the compressor is to raise the intake pressure; this way, the engine will "breathe" more, increasing the filling of the dense air in the cylinders. [1] An engine's performance increase depends on a compressor's ability to compress the air without adding excess heat. Increased pressure will have a function of two variables: temperature and air density, but only the increase in air density allows more fuel to burn and therefore increases the power of the engine. The bearing system supports a shaft that connects the turbine and compressor together. The bearing system has many purposes in the turbocharger. In addition to reducing the friction energy losses that are obtained from the turbine and required to bring the compressor to a working state, it must also provide stability for various working conditions. The bearing system is affected by not a single force: thrust, which is caused by the pressure difference between the turbine and the compressor; the various radial forces caused by the uneven torque rate of the engine; and thermal load, which is mainly caused by exhaust gases and high rotational speeds. Most of the turbocharger bearing systems are journal bearings made of bronze; they have a hydrodynamic oil lubrication system, but to protect lubricating oil from exhaust gas high temperatures Bearing housings have water jackets, gas seals, and other design features [1]. The turbocharger working principle is based on using the exhaust gases produced by the engine, which otherwise would be wasted energy. Exhaust gases travel through the exhaust manifold, and in the form of heat and pressure, they enter the turbine stage. Due to the back pressure and the heat expansion against the turbine wheels caused by the turbine housing, it causes the wheels and shaft to spin [1]. Consequently, this induces the compressor wheel to rotate. The remaining exhaust gases leave the turbocharger system and enter the exhaust pipes. Due to the rotation from the intake side of the system, air is sucked in to the compressor stage where it is being compressed, increasing the density and the temperature of the air, but before this hot pressurized air goes into the engine's cylinders, it must be cooled; therefore, air passes through the intercooler section, which further increases the density while cooling the air down. After the cooling air has traveled through another tube from the cooler's discharge side to the engine's intake manifold, where the air is distributed into the individual cylinders. In the cylinders now with a denser air and fuel mixture, combustion happens after the combustion exhaust passes through the exhaust valve into the exhaust manifold, and the cycle repeats. During these processes, the turbocharger is exposed to a different type of structural-thermal load.

2. Types of bearings in stationary turbochargers (journal bearing) short review

The bearings in stationary turbochargers are essential for maintaining the rotating shaft's stability and enabling extremely high rotation rates. Turbochargers generally use one of two types of bearings:

Thrust Bearings

Thrust bearings account for axial loads, indicating that this type of bearing manages forces acting along the length of the shaft. The thrust bearing prevents the rotor from moving axially and maintains its place along the shaft. These bearings are usually lubricated with oil and come in a variety of designs, including single and double direction thrust bearings.

Journal Bearings

A journal bearing is a kind of bearing that enables a turbocharger's rotating shaft to move with reduced friction inside a bearing surface. Because the shaft of a turbocharger rotates at incredibly high speeds, often over 100,000–150,000 RPM. The journal bearing's design is essential to provide long-term performance, minimize wear, and supply enough lubrication [2],[3].

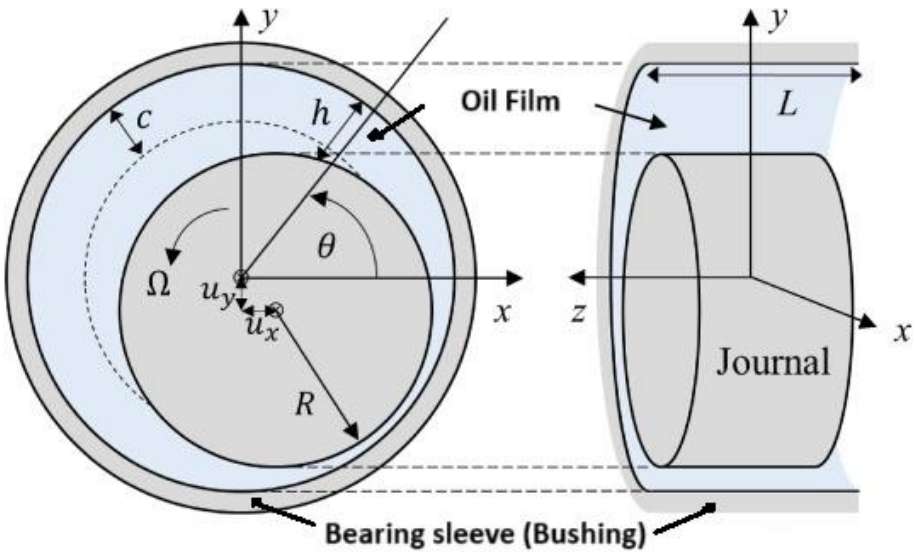

Figure 1. Schematic description of Journal bearing [4].

In Figure 1, a schematic description of journal bearing components is presented.

The journal is the rotating part of the shaft that makes contact with the bearing surface. This part in turbochargers spins within the bearing supported by lubricating fluid, commonly a thin film of oil. The **bearing sleeve (bushing)** is the stationary part surrounding the journal (rotating shaft). **Oil film** forms between the journal and the bearing sleeve; this oil film prevents direct metal-to-metal contact, which reduces friction and wear. It's maintained by the turbocharger's lubrication system, which provides pressurized oil to the bearing. Additionally, the journal bearing has an oil feed hole to supply pressurized oil to create the lubrication film and an oil drain hole to return used oil back to the special oil reservoir.

On the figure 1, h represents film thickness, which can be expressed as:

$$(1)\ h = c - u_x\, cos(\theta) - u_y\, sin(\theta).$$

Where c denotes the clearance, u_x and u_y are the eccentricity of the journal along the x and y axes, respectively [4].

The working principle of a journal bearing is based on hydrodynamic lubrication. When the shaft (journal) rotates inside the bearing sleeve, the motion of the shaft helps lubricating oil to enter into the bearing gap (oil feed hole). This action forms a thin, continuous oil film, which separates the shaft from the bearing surface, supports it, and reduces friction. As long as the shaft rotates at a sufficiently high speed and there is enough oil pressure, the journal bearing is said to be operating under hydrodynamic lubrication, where contact between two metals is avoided.
Commonly used materials for journal bearings are copper-based alloys for their excellent wear resistance and ability to conduct heat away from the bearing and bronze alloys due to their good durability and strength [2, 3].

Additionally, ceramic or ball bearings can be used for the high-performance turbochargers; compared to traditional journal bearings, ball bearings offer advantages like reduced friction, faster spool-up times, and better durability under extreme conditions. These bearings are increasingly used in more advanced and high-efficiency turbochargers, including both stationary and automotive turbochargers.

3. Heat Transfer in Turbochargers, obtaining the HTCs.

Understanding heat transfer within turbochargers is essential for optimizing their design and functionality. Effective management of thermal loads can prevent overheating, reduce thermal stress, and improve the longevity of turbocharger components. This involves a complex interplayof conduction, convection, and radiation processes that affect various parts of the turbocharger, from the turbine and compressor wheels to the housing and bearings.

In order to correctly estimate the heat transfer in a turbocharger, an accurate estimate of the enthalpyin the working fluid is required, as it has a direct impact on the performance and efficiency of the system. According to the source [5], the heat transfer process in turbochargers is complex, occurring in a three-dimensional space and influenced by various factors including the turbocharger's configuration (such as size, cooling methods, and materials) and the surrounding environment (like engine proximity, packaging, and operating conditions). Therefore, the compressor and turbine sections are significantly affected by heat transfer dynamics. As the fluid undergoes compression or expansion, changes in pressure lead to temperature variations, which are closely tied to the entropy changes of the gas between different states. Understanding these interactions is essential for optimizing turbocharger performance and ensuring reliable operation under varying conditions. This effect can best be shown by the entropy formula, which describes

the change in entropy of a gas between two states:

$$(7)\ S_2 - S_1 = c_\mathrm{p}\, ln\left(\frac{T_2}{T_1}\right) - \mathrm{R}ln\left(\frac{P_2}{P_1}\right), \text{ or } (8)\ S_2 - S_1 = c_\mathrm{v}\, ln\left(\frac{T_2}{T_1}\right) + \mathrm{R}ln\left(\frac{V_2}{V_1}\right) [5].$$

Depending on a process (1) equation is used when we have constant pressure process and (2), when there is a constant volume process. c_v and c_p in the equation represents specific heat capacities at constant volume and pressure, respectively; R is the universal gas constant. 8.3144598 Numbers 1 and 2 indicate states at the beginning and end of the compression process, *S* is the entropy, *T* is the temperature, *P* is the pressure, and the term "ln" denotes a natural logarithmic function. If we divide both equations by the mass of gas, we will get specific forms of the given equations. For simplicity, the first term of the equation reflects the contribution of the constant pressure/volume process, while the second term represents the contribution of the additional change produced by the non-constant pressure/volume condition.

For the $S_2 - S_1 = 0$ equation becomes:

$$(8)\ c_\mathrm{p}\, ln\left(\frac{T_2}{T_1}\right) = \mathrm{R}ln\left(\frac{P_2}{P_1}\right).$$

Furthermore, if we divide both sides with C_p the equation will be in the form of:

$$\left(\frac{T_2}{T_1}\right) = \left(\frac{P_2}{P_1}\right)^{\left(\frac{R}{c_\mathrm{p}}\right)}.$$

Since $c_\mathrm{p} - c_\mathrm{v} = \mathrm{R}$. from the definition of specific heat coefficients and $\frac{c_\mathrm{p}}{c_\mathrm{v}} = \gamma$ The ratio between specific heat coefficients: $\frac{R}{c_\mathrm{p}} = 1 - \frac{1}{\gamma} = \frac{\gamma-1}{\gamma}$.

Finally, the equation becomes: (9) $\left(\frac{T_2}{T_1}\right) = \left(\frac{P_2}{P_1}\right)^{\left(\frac{\gamma-1}{\gamma}\right)}$. According to this equation, during the compression process when P_1 increased to P_2 the temperature increases from T_1 to T_2, the Constant γ depends on the origin of the gas; for air at standard conditions, the value of γ is 1.4. And the exponential term becomes 0.286. Therefore, if the pressure doubled during the compression, the temperature would increase approximately by 1.219 times. Thus, it is a function that connects together temperature and pressure changes during the compression process [5].

By substituting the state equation of the gas ($PV_\mathrm{vol} = m\mathrm{R}T$) and if $m = 1(\mathrm{kg})$: $PV_\mathrm{vol} = \mathrm{R}T$ (where V_vol is the specific volume occupied by the gas) into the equation (3):

$$(10)\ \left(\frac{P_2 V_{\mathrm{vol},2}}{P_1 V_{\mathrm{vol},1}}\right) = \left(\frac{P_2}{P_1}\right)^{\left(\frac{\gamma-1}{\gamma}\right)}.$$

By multiplying both sides to $\left(\frac{P_1}{P_2}\right)$:

$$(11)\ \left(\frac{P_2}{P_1}\right) = \left(\frac{V_{\mathrm{vol},1}}{V_{\mathrm{vol},2}}\right)^{\gamma}.$$

With the help of this equation, it is possible to determine change in pressure according to the given

compression ratio $\left(\frac{V_{\text{vol},1}}{V_{\text{vol},2}}\right)$.

For analyzing heat transfer processes in turbochargers, it's important to acknowledge that realheat addition and removal occur continuously, making discrete modeling an oversimplification. However, the enthalpy-entropy (*h*-*S*) diagram offers a useful starting point for both qualitative and quantitative assessments. The *h*-*S* diagram, also known as the enthalpy-entropy diagram, is a graphical representation used in thermodynamics to analyze and visualize the thermodynamic processes of fluids, typically used for steam and refrigeration cycles. It plots enthalpy (*h*) on the vertical axis and entropy (*S*) on the horizontal axis. The h-S diagram helps visualize and evaluate the stages of heat transfer by showing how enthalpy changes with entropy, allowing for more precise calculations of heat addition and removal. This approach provides valuable insights into the performance and efficiency of turbochargers [5].

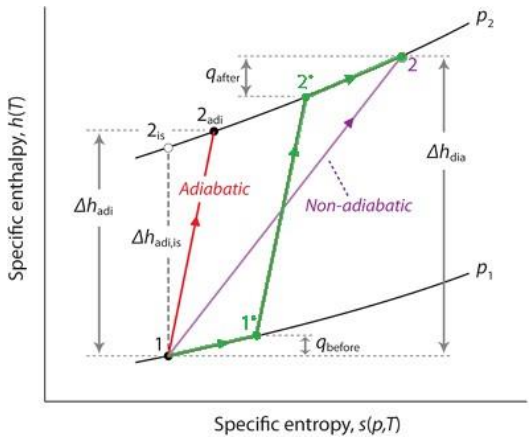

Figure 2. TC Compressor h-S diagram [5].

Figure 2 shows the compression process in the turbocharger from P_1 to P_2 pressure. Different colors on the graph indicate, different processes by which compression can occur. If theprocess is adiabatic, the final state of the working fluid will be denoted with 2_{adi}, the path will be $1 \rightarrow 2_{\text{adi}}$ (red line). However, if the process is diabatic and, for example, heat addition is present in a system, the final state will be different from 2_{adi} point. The new path will be $1 \rightarrow 2$, denoted with the purple line. According to the source [5], the compressor process inside the compressor wheel generally is assumed to be adiabatic, but some researchers consider heat addition to be present before and after compression. Also, there are researchers who think that heat addition occurs only after the compression process. The first assumption is illustrated on the graph, by the path $1 \rightarrow 1^* \rightarrow 2^* \rightarrow 2$ (green line). $1 \rightarrow 1^*$ and $2^* \rightarrow 2$ show the result of heat addition before and after the

compression process (q_{before} and q_{after}), which further increases the temperature. The process $1^* \rightarrow 2^*$ indicates the adiabatic compression between P_1 and P_2 constant pressure curves. Dividing a complex heat transfer process into simple, specific areas with their own corresponding heat transfer processes has a great positive side, which is easily detecting heat removal or addition with the help of the enthalpy change. Furthermore, with information provided by [5], the context of a compressor, the change in enthalpy Δh is a key parameter used to evaluate the performance and efficiency of the compressor. The efficiency of a compressor is often assessed by comparing the actual work input to the ideal work input based on the enthalpy change. Generally, the equation of adiabatic efficiency is given by the formula:

$$(12)\ \eta_{\text{adi.c}} = \frac{Isentropic\ work\ input}{Actual\ work\ input}.$$

Where the isentropic work input is based on the ideal (isentropic) enthalpy change, while the actual work input is based on the real process enthalpy change. For an isentropic process, the change in enthalpy $\left(\Delta h_{\text{adi,is}}\right)$ Is calculated from the ideal (isentropic) process: $W_{\text{is}} = h_{2,\text{is}} - h_1$.. The actual work input is based on the real enthalpy change: $W_{\text{act}} = h_2 - h_1$. Therefore, the equation will take the following form:

$$(13)\ \eta_{\text{adi.c}} = \frac{\Delta h_{\text{adi,is}}}{\Delta h_{\text{adi}}} = \frac{T_{2,\text{is}} - T_1}{T_{2,\text{adi}} - T_1}.$$

If we also take into account, the heat transfer during the compressor process (diabatic efficiency):

$$(14)\ \eta_{\text{diab.c}} = \frac{\Delta h_{\text{adi,is}}}{\Delta h_{\text{diab}}} = \frac{T_{2,\text{is}} - T_1}{T_2 - T_1}.$$

The same approach can be used in the turbine wheel; similarly, during the expansion process, the assumption can be heat removal before and after expansion; therefore, the process can be divided intothree stages. in figure 4, the following process is described by the green lines $3 \rightarrow 3^* \rightarrow 4^* \rightarrow 4$. Path $3 \rightarrow 3^*$ on the constant pressure curve P_3 indicates heat removal before the expansion process. The adiabatic expansion is represented by the path $3^* \rightarrow 4^*$, and the final stage is $4^* \rightarrow 4$ where additional heat removal occurs on the constant pressure curve, P_4 after the expansion process.

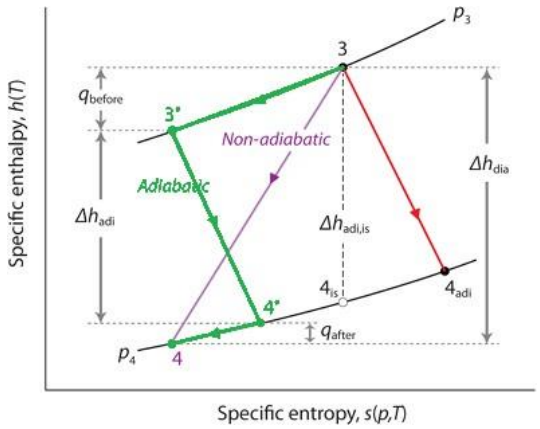

Figure 3. TC Turbocharger *h-S* diagram [5].

As for the adiabatic efficiency in the turbine wheel, similarly to the compressor, it is expressed by the formula:

$$(15)\ \eta_{\mathrm{adi.T}} = \frac{\Delta h_{\mathrm{adi}}}{\Delta h_{\mathrm{adi,is}}} = \frac{T_3 - T_{4,\mathrm{adi}}}{T_3 - T_{4,\mathrm{is}}}.$$

If we want to include heat transfer in the turbine wheel, diabatic efficiency formula will take the following form:

$$(16)\ \eta_{\mathrm{diab.T}} = \frac{\Delta h_{\mathrm{diab}}}{\Delta h_{\mathrm{adi,is}}} = \frac{T_3 - T_4}{T_3 - T_{4,\mathrm{adi}}}.$$

However, based on [5], the fact that $T_4 < T_{4,\mathrm{adi}}$, diabatic efficiency will be higher than adiabatic, which is not physically feasible. The problem is that based on assumptions, the heat is removed before expansion, which causes the graph to shift toward lower entropy than in the isentropic case $\Delta h_{\mathrm{diab}} > \Delta h_{\mathrm{adi,is}}$. but we should take into account that equation (16) does not include the work done against mechanical friction losses. Therefore, to properly determine the turbine's diabatic efficiency, it is essential to directly measure the shaft power.

4. Heat transfer in turbocharger

For better understanding of heat transfer in turbochargers, a review of figure (4), which represents a longitudinal section of a simplified turbocharger model, with highlighting the primary heat transfer pathways, will be used. Main mechanisms of heat transfer in TC are conduction, convection, and radiation. Firstly, exhaust gases coming from the engine coming from combustion into the turbine exchange heat by forced convection to the turbine casing and bearing housing ($(Q_{\mathrm{t}\to\mathrm{BH}}$). After this, due to the temperature difference between the turbine casing's inner and outer surfaces, heat transfers via conduction through the wall and dissipates by natural convection $(Q_{\mathrm{T,conv}})$ plus radiation $(Q_{\mathrm{T,rad}})$. Meanwhile, exhaust gases continue to travel through turbine blades, causing the air to expand, pressure to drop, and temperature to decrease. during this, heat is transferred to the blades and consequently to the shaft $(Q_{\mathrm{T}\to\mathrm{S}})$.

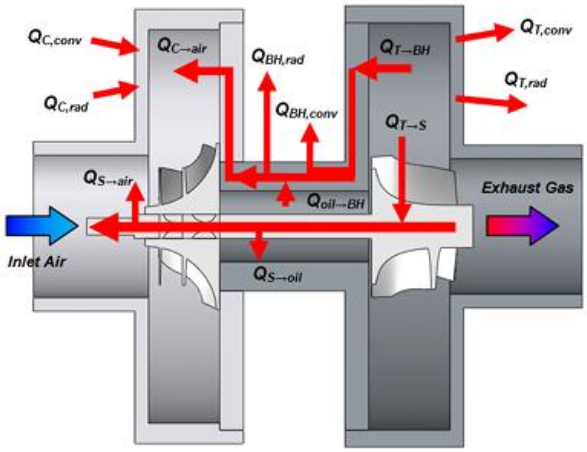

Figure 4. Section-view of reduced order heat transfer model in TC [5].

While the exhaust gases expand in the turbine, cold air enters the compressor. But because the shaft is already heated from exhaust gases, it causes inlet air to heat up $(Q_{\mathrm{S}\to\mathrm{air}})$. During the compression process in the compressor wheel, air temperature and pressure rise. After compression, the air moves into the diffuser, where it is further heated by forced convection from the back plate $(Q_{\mathrm{C}\to\mathrm{air}})$. Similarly, to the turbine side, conductive heat transfer happens through the casing wall due to the temperature gradient, and finally, with natural convection $(Q_{\mathrm{C,conv}})$ and radiation $(Q_{\mathrm{C,rad}})$, heat dissipates into the surrounding environment. On the other hand, in the bearings housing, heat is transferred to the oil through forced convection $(Q_{\mathrm{oil}\to\mathrm{BH}})$, but also through free convection $(Q_{\mathrm{BH,conv}})$ and radiation $(Q_{\mathrm{BH,rad}})$. As for the shaft, heat is transferred only by forced convection to the oil $(Q_{\mathrm{S}\to\mathrm{oil}})$. Heat generation due to friction within the bearing housing is neglected in this model.

4.1. Obtaining the HTC. Formula.

Firstly, the heat transfer coefficient (h) for compressor and turbine volutes is typically derived using a combination of empirical correlations, theoretical fluid dynamics principles, and experimental data. The volutes are complex geometries where fluid is subjected to swirling and varying pressure conditions, which complicates the heat transfer process. However, a general approach involves the following steps:
Heat transfer in volutes primarily occurs with **convection** between the fluid and the wall and is a function of the local temperature difference and flow conditions. From the basic principle of heat transfer, the HTC. can be derived from the following general formula for forced convection:

$$Q = hA\Delta T.$$

Where: Q is heat transfer rate, h is heat transfer coefficient, A is the heat transfer area, and ΔT is the Temperature difference between the fluid and the wall.

The heat transfer coefficient is usually derived through correlations involving the **Reynolds number** (Re) and the **Nusselt number** (Nu). These correlations are often based on experimental data or numerical simulations for similar geometries.

$$Nu = a\, Re^{b} Pr^{c} \text{ [6].}$$

Where: $Nu = \frac{hL}{K}$ is Nusselt number, $Pr = \frac{\nu}{\alpha}$ is Prandtl number which approximates the ratio between kinematic viscosity to thermal diffusivity, $Re = \frac{V\,D}{\nu}$ is Reynolds number, dimensionless quantity that measures the ratio of inertial forces to viscous forces in a fluid flow. a , b and c are the arbitrary constants. L and D is characteristic length, V is velocity [6]. In practice, **empirical correlations** or **numerical simulations** are often used to determine heat transfer coefficients for volutes, as the flow in these components is highly three-dimensional and influenced by complex factors such as laminar to turbulent flow, swirl, and curvature effects. For low-Reynolds number flow, a laminar flow model might be used, but in most compressor and turbine volutes, the flow is turbulent, and models based on turbulent flow correlations, such as those from Dittus-Boelter [7] or Gnielinski [8], are more appropriate. In terms of swirl and curvature effects, swirling motion of the fluid in the volute creates complex heat transfer patterns that are not easy to model analytically. The presence of centrifugal forces, variations in pressure, and the curved geometry of the volute mean that both radial and tangential components of the flow contribute to the heat transfer process. Additionally, there are temperature gradient effects; the temperature in a turbine or compressor volute will differ from the core flow temperature due to heat exchange with the environment and potential internal heat generation. In a compressor, the temperature will typically increase due to compression and friction, while in a turbine, the temperature will drop due to expansion and work extraction. In both cases, the heat transfer coefficient can be highly dependent on the local temperature gradient, which can vary along the volute [9]. Luckily, authors A. Romagnoli and Ricardo Martinez-Botas suggested a formula for HTC, for a simplified model of compressor and turbine volute, where they use the Dittus-Boelter correlation and the volute is modeled as a straight pipe; the heat transfer coefficient can be calculated from the Nusselt number when D/2 is chosen for the characteristic length:

$$h_{\mathrm{t,c}} = Nu\frac{2K}{D} = 0.046\frac{K}{D}\, Re^{0.8} Pr^{0.4} \text{ [5].}$$

In the case of a shaft, heat transfer by convection is modeled as flow in an annular gap between two cylinders; for this state, the formula to provide the heat transfer coefficient is suggested by [10] Tachibana F, Fukui S. They conducted the experiments about heat transfer by convection in an annular gap between a rotating inner cylinder and a stationary outer cylinder. Firstly, Tachibana F, Fukui S. prepared the experiment. The setup consists of four types of apparatuses. One type, referred to as (A), features stationary inner and outer cylinders. The remaining three types have a rotating inner cylinder and a stationary outer cylinder that is either heated or cooled. Among these, type (B) has a heated inner cylinder and an outer cylinder cooled by water. Types (C) and (D) both have cooled inner cylinders, but their outer cylinders are heated. They describe the experiment in detail, saying that the flow velocity ranges from 4 to 32 m/s. The experiments were carried out on the 4th and 5th sections, located 70 mm from the leading edge of the inner cylinder. Surface temperatures were measured using a copper-constantan thermocouple, which was soldered to the inner cylinder at three points: the center and both sides of each section. The electrical input to the heater was adjusted to maintain a uniform temperature difference between adjacent cylinders at their joint. The heat flow for each cylinder is determined based on the electrical input. The air temperature is recorded as the average value measured by thermocouples at the inlet and outlet. The heat transfer coefficient is calculated by dividing the heat flow by the surface area of the cylinder and the temperature difference between the cylinder and the air. The heat dissipated through radiation is calculated separately and subtracted from the total. Schematic diagram of One of the apparatuses, named (B) (closest to the turbocharger shaft), is shown in the figure below:

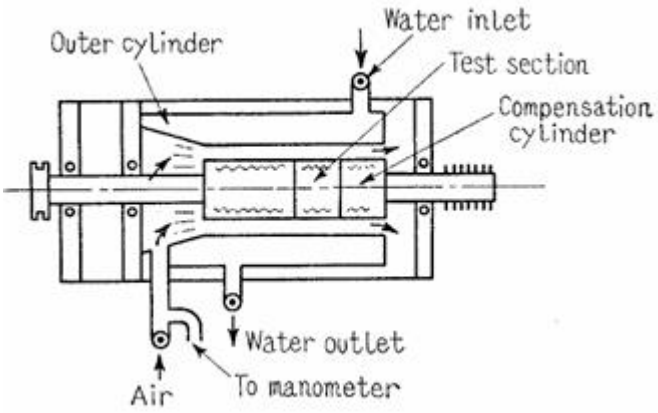

Figure 5. Schematic diagram of experimental equipment (B) [10].

Based on [10], figure 5 indicates the test apparatus (B), which has a heated inner cylinder with an outer diameter of 120 mm and a length of 45 mm. Two temperature-compensation cylinders, both matching the diameter of the test cylinder, are positioned coaxially on either side of the inner cylinder. One compensation cylinder is placed upstream and has a length of 190 mm, while the other is downstream and 45 mm long. Each compensation cylinder is equipped with a heater made of insulated nichrome wire. The outer cylinder is fitted with a water-cooled jacket, and its inner diameters are 128 mm, 136 mm, 144 mm, and 160 mm. To measure temperature, a thermistor is mounted on the surface of the rotating inner cylinder. Thermocouples are used to measure the temperature differences between the test cylinder and the compensation cylinders, as well as the temperature of the stationary outer cylinder. The air temperature is recorded by thermocouples

located at the inlet and outlet of the annular gap. The mean axial flow velocity is calculated based on the flow rate, which is measured at an orifice.

After the experimental results, Tachibana F. and Fukui S. developed the equations for the turbulent heat transfer in annuli. They say that there are many investigations on heat transfer of turbulent flow in annuli; however, in many past studies the outer cylinder is insulated, whereas the experiment mentioned above suggests that the outer cylinder is heated or cooled (depends on apparatuses (A, B, C, D). Additionally, the test section is positioned near the beginning of the heating process, which results in higher heat transfer coefficients. Given these factors, the test sections are divided, and local heat transfer coefficients are calculated. Finally, they obtained two Nusselt number formulas, one for both sides heated:

$$(19)\ Nu = 0.017Re^{0.8}Pr^{\frac{1}{3}}\left(1 + 2.3\frac{D_e}{L}\right)\left(\frac{D_2}{D_1}\right)^{0.45}\ [10].$$

And for one side heated and other cooled:

$$(20)\ Nu = 0.015Re^{0.8}Pr^{\frac{1}{3}}\left(1 + 2.3\frac{D_e}{L}\right)\left(\frac{D_2}{D_1}\right)^{0.45}\ [10].$$

From the equations and also from the graph below (figure 3), which shows the difference between the coefficients of heat transfer when inner and outer cylinders are heated and those of heat transfer when the one is heated and the other is cooled. The difference between these two equations is not much; in fact, either of them can be implemented in the corresponding turbocharger analysis, but since oil is used as a coolant in TC, the outer surface of the "cylinder" in this case will be cooled and the inner (the TC. Pin) will be the heated "cylinder"; therefore, equation 20 will be used in the analysis.

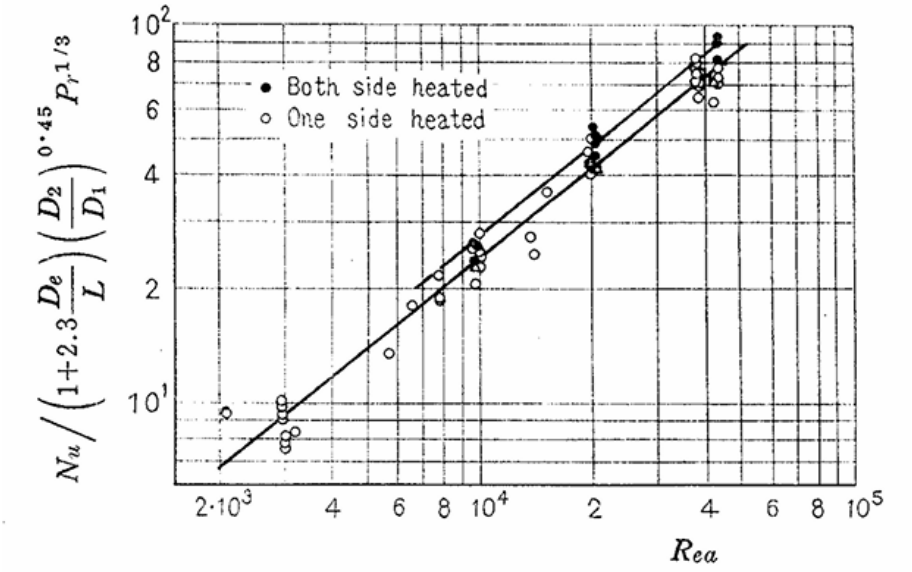

Figure 6. Turbulent HT. in annuli [10].

On the figure 6. Abscissa indicates Reynolds number and ordinate shows Nusselt number divided by product: $\left(1 + 2.3\frac{D_e}{L}\right)\left(\frac{D_2}{D_1}\right)^{0.45} Pr^{\frac{1}{3}}$.

5. Bolt pretension.

Bolt connections are the crucial and most important places in the structure since that is where the weakest places in the structure are. With this in mind, great attention should be given, and carefully chosen sizing, tension, placement, etc. Numerous parts of the turbomachinery, such as pipes and housings, have to be disconnected or dismantled. Although bolted connections appear simple and provide separation, their mechanical behavior, performance, and operation can be complicated. Bolted connections should only be used for disassembly or adjustment for operation or maintenance due to their typically highly non-linear and complex behavior. Bolt connections also require special care and precautions such as inspection, maintenance, etc., and are more costly than welding and other types of connections. Furthermore, screw connections are heavy. Bolt connections make up a very small portion of a turbomachine's total cost. On the other hand, they are accountable for numerous problems that can occur during the operation, issues with leaks, malfunctions, and shutdowns. The dimensions and layout of attached components, modules, and subsections are frequently dictated by bolt-connection specifications. In a bolt connection, there are numerous parts. Specifics of the bolts (size, patterns, etc.). Bolt connection performance and reliability are greatly impacted by the following factors: application and specifics of nuts and washers; connecting plates and components; and main connected assemblies. Damage to each of the above components can lead to several different failures. Cracks may occur due to the load, damage at the location of bolt holes, or the failure of the structure due to the bending moment [11]. In his work, author Amin Almasi writes that significant difficulty and complexity in bolt connections are local yielding in different parts. This involves localized loads and highly localized stresses, also high nonlinearities. For example, nonlinearity due to stress-strain relationships and the involvement of complex contact and contact stresses. The bolt connection exhibits increasingly complex and nonlinear behavior as components yield and plastic zones expand. Bolt load (plastic) redistributions occur after some yielding and typically result in a reduction in stiffness and an increase in the bolt connection's moment capacity. The redistribution of bolt loads and forces, however, is a complicated phenomenon. There are many theories and modern approaches, but it is still a problem to accurately predict the behavior of bolt connections. Before we bring the turbocharger to a working state, we need to tighten the bolts. This is a very important part of making sure the structure is tight, and the parts that transmit the load to the parts that take this force on themselves are well connected to each other. Bolts might be re-tightened as well if the bolts have been adjusted and loosened. Since we know that the connection of the bolts is quite strong, rigid, and durable and will ensure the protection of the structure from rupture, the connection of the parts with as little gap as possible to prevent leakage, Amin Almasi in his work suggests that we must not forget areas of concerns about bolt connections and keep them in mind, it might be; the gradually loosening the connection over time, a large amount of bolt load loss can be occurred withing the few days or weeks after the tensioning, slip resistance of the joints and washer requirements, their importance is acknowledged since, typically bolt connection with washers results preload loss to be between 6-14% depending on a number of washers used. (10-15 years of operation). We must not forget that in addition to all the different loads in the turbomachinery, there is also a vibration caused by dynamic oscillations. Accordingly, it is necessary to pay attention to the connection of the bolts. To avoid the risks of its

propulsion during cystic and dynamic loads Nuts in the bolt connections must be additionally secured. Bolt connection is one of the weakest links in the structure; therefore, we have to consider optimal spacing between centers of the bolts in order not to further weaken the structure and avoid failure. From the Amin Almasi work, he indicates that optimal spacing between the bolt centers should be 2.5 times the bolt hole diameter, and the edge distance, to be safe, should be 1.75 - 2 times the diameter.

6. Other Approaches for Similar Problems (A Review of Current Field Analysis).

Thermal and structural analysis of turbochargers is critical for ensuring performance, reliability, and longevity. Since turbochargers operate in extreme conditions (high speeds, temperatures, and pressures), both types of analysis help identify potential issues such as thermal stresses, material degradation, and deformation. There are various approaches for conducting these analyses, which can be broadly categorized based on computational methods, experimental techniques, and hybrid methods. Some of the acknowledged methods are Finite element analysis (FEA) - is one of the most common numerical methods for thermal and structural analysis. It helps simulate heat transfer, convection, radiation, and conduction within turbocharger components. In structural analysis, it can simulate how the turbocharger components will deform under mechanical stresses, such as centrifugal forces, thermal expansion, and vibration. Computational Fluid Dynamics (CFD) - is mainly used to simulate the fluid flow, heat exchange, and thermal performance within the turbocharger. It models how exhaust gases or intake air behave thermally during high-speed operation. These methods are often used together to solve thermo-structural problems. Typically, the CFD part solves fluid flow and convection, while the FEA part solves heat conduction and other mechanical phenomena in solids. These simulations can be strongly coupled (thermal-mechanical coupling) or weakly coupled, depending on the problem. Weak coupling is when the CFD and FEA simulations are solved separately, with results from one domain (e.g., temperature) fed into the other (e.g., structural analysis), whereas Strong coupling: Thermal effects from the CFD simulation directly influence structural behavior in FEA, and mechanical deformations in the solid domain are passed back to affect fluid flow in the CFD domain. This hybrid method is useful for steady and also transient operating conditions. The CDF + FEA method is further discussed in [12]. P. Luczynski, M. Giesen, T. Gier and M. Wirsum work. They proposed different (CFD+FEA) methods for transient state thermo-structural analysis of turbochargers and compared their accuracy and computational time to each other and to (CHT) conjugated heat transfer. Which is a numerical method typically used in simulations that involve both solid bodies (e.g., a metal plate) and surrounding fluids (e.g., air or water). These simulations require solving the heat transfer equations in both the solid and fluid regions simultaneously, and they must account for the boundary conditions where the two regions meet, as heat is transferred between them [13]. Firstly, in their article (P. Luczynski, M. Giesen, T. Gier, M. Wirsum), they provided a thermal shock test for the purpose of thermo-mechanical analysis [14]. Thermal shock is simplified equivalent to the real driving cycle when the turbine inlet temperature changes drastically, and therefore maximum thermal stress arises. The figure shown below depicts the fluid inlet temperature to a turbocharger rapidly changing with a step function. The time-dependent,

logarithmic increase in solid body temperatures during thermal shock occurs between the cold turbine condition at operating point 1 (OP1) and the hot turbine condition at operating point 2 (OP2). Thermocouples on the turbine wheel (TW) and turbine housing (TH) are presented to monitor temperature change. Further description is given in [12].

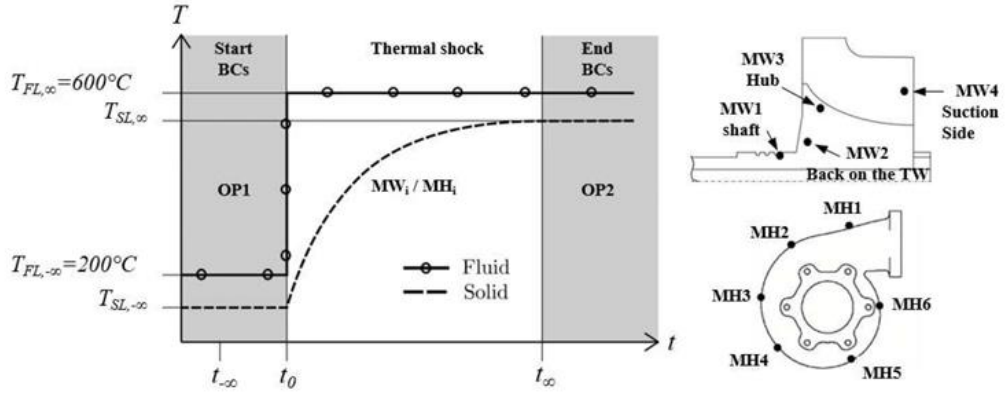

Figure 7. position of the thermocouples on turbine wheel and turbine housing (right), Schematic plots of temperature in a heating thermal shock (left) [12].

The main uncoupled CFD FEA methods provided by paper [12] are the simple Bulk Temperature (BT) method, the Analytic Adiabatic Y-plus (AAY) method, the Diabatic Y-plus Field (DYF) method, and the Temperature Influence Coefficient (TIC) method. All of these approaches are integrated with the TFEA-EXPO interpolation method. TFEA-EXPO interpolation is a method used for solving interpolation problems, particularly in numerical simulations or when approximating data points. It stands for **Tensor-Flow Element-wise Adaptive-EXPO**; the exact implementation can vary depending on the context. TFEA-EXPO interpolation aims to provide accurate approximations for data that exhibit exponential trends or when there are complex, nonlinear relationships between data points. [14]. The figure from the article provided by P. Luczynski, M. Giesen, T. Gier, and M. Wirsum shows thermo-structural analysis on the turbocharger turbine wheel and housing using different CFD FEA approaches.

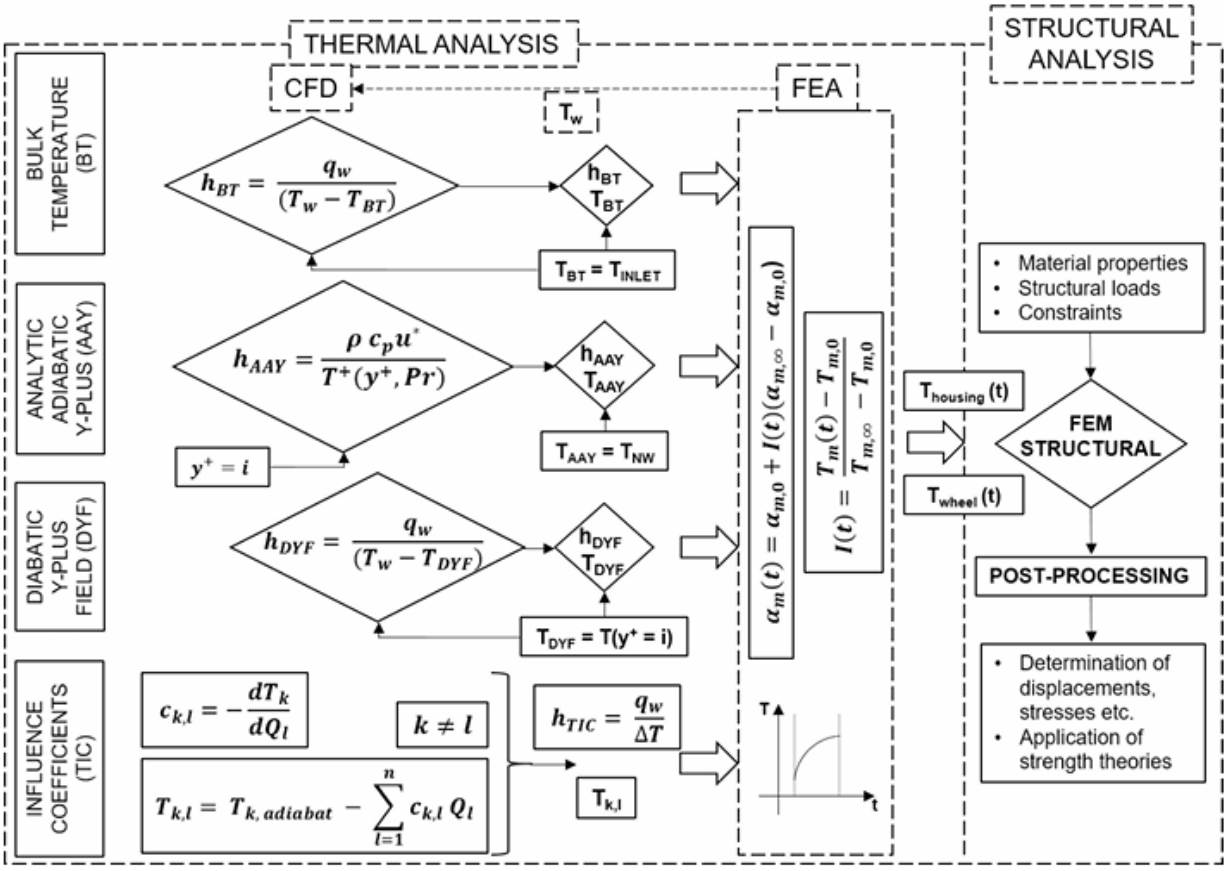

Figure 8. Flow chart of thermo-structural analysis using various CFD-FEA approaches.

In the BT (bulk temperature) approach, a constant bulk temperature (T_{BT}) is chosen as the reference temperature for the fluid, which is set equal to the fluid temperature at the turbocharger inlet in their investigated case. more information [12]. However, using T_{BT} in this method can lead to inaccuracies in modeling the local heat transfer through the thermal boundary layer. The thermal boundary conditions for diabatic CFD simulations are estimated to be approximately 90-99% of the inlet air temperature.

The AAY (Analytic Adiabatic Y-plus) method utilizes a straightforward adiabatic CFD calculation and employs an analytical definition of the heat transfer coefficient (HTC) derived from dimensionless boundary layer equations. It demonstrates that heat transfer coefficients remain constant for higher y^+values equal to i. To reduce errors in HTC caused by inaccurate thermal boundary conditions, the method calculates the heat transfer coefficients (h_{AAY}) using a non-dimensional temperature located further from the viscous sub-layer ($T^+(y^+, \mathrm{Pr})$). In adiabatic simulations, the near-wall temperature (T_{NW}) serves as the fluid reference temperature, with the assumption that the temperature difference between T_{NW} and the fluid temperature at the thermal boundary layer's edge is negligible.

In the DYF (Diabatic Y-plus) approach, the heat transfer coefficient (HTC) is calculated using a defined simple equation:

$$(21)\ h_{\mathrm{DYF}} = \frac{q_{\mathrm{w}}}{(T_{\mathrm{w}} - T_{\mathrm{DYF}})}\ [12].$$

This equation is also one of four main iteration schemes between CFD and FEA solvers called (hFTB) heat transfer coefficient front temperature back. During the iteration process, the resulting wall temperature is sent back from the FEA solver to the CFD simulation, which is how the hFTB method got its name [12]. and the fluid reference temperature (T_{DYF}) is determined from the local fluid temperatures at a distance of $y^+ = i$ from the diabatic wall. This method takes advantage of the similarity between velocity and temperature profiles in turbochargers to model the thickness of the thermal boundary layer. Like the BT method, wall temperatures for CFD simulations are approximated to be about 90-99% of the inlet air temperature.

The TIC (influence coefficients) approach was originally created to analyze windage and heat transfer in rotor-stator cavities. Essentially, this method splits the relevant surfaces into several zones for heat transfer analysis. Multiple adiabatic and diabatic CFD simulations are conducted to determine the heat transfer coefficients and reference fluid temperatures. The main objective of the method is to capture the heat transfer interactions between individual surfaces using influence coefficients ($C_{k,l}$), which are then used to calculate the reference fluid temperatures.

From the analysis conducted by P. Luczynski, M. Giesen, T. Gier, and M. Wirsum, it is evident that all four uncoupled CFD-FEA methods mentioned above performed relatively well and showed promising results compared to experimental data. The analysis of the turbocharger shows that the BT method has a relatively low error between measured and simulated values of temperature. with averaged RRMS (Relative Root Mean Square) errors being 3.33% in the turbine wheel (TW) and 5.48% in the turbine housing (TH). The main drawback of this method is the lack of physical correlation between fluid reference temperature and local heat transfer. In the case of the Analytic Adiabatic Y-plus (AAY) and Diabatic Y-plus Field (DYF) methods, since they consider the local displacement thickness of the thermal boundary layer. The setup of both approaches depends on the value of the dimensionless wall distance y^+. Therefore, simulations with higher y^+ values achieved more precise results, with averaged RRMS error in TH equal to 1.26% (AAY, $y^+ = 250$), 1.13% (DYF, $y^+ = 250$). In TW average RRMS error – 4.42% (AAY, $y^+ = 250$), and 1.37% (DYF, $y^+ = 250$). Also, the TIC method showed good agreement with experimental data – an averaged RRMS error of 1.05% in TH and of 4.90% in TW. However, the accuracy of the Temperature Influence Coefficient method is strongly dependent on the experience of the user. Identifying the walls with similar heat transfer conditions and correctly defining the surfaces with their respective temperature influence coefficients can be challenging and difficult. Moreover, since the TIC method splits model surfaces into multiple zones, the additional division of walls into smaller surfaces would increase the quality of the results, but it will increase computational effort due to the requirement of several CFD simulations. Additionally, these methods are relatively fast; approximately 60% computational time reduction can be achieved relative to coupled simulation with desired accuracy [12].

6.1. Analytical Approach. Lumped capacity method 1-D, 2-D.

Another approach to model heat transfer through turbocharger is using 1-D or 2-D models, one of the common methods to create 1-D heat transfer models is lumped capacitance method.

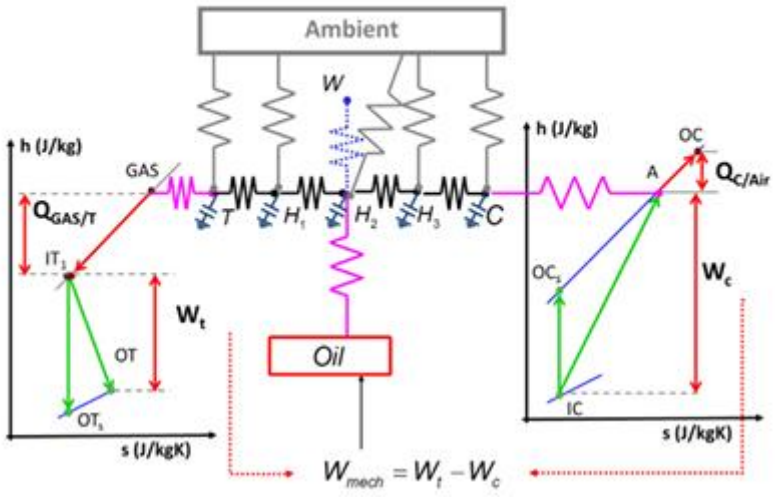

Figure 9. 1-D lumped capacitance model [13].

A lumped capacitance model is a simplified representation that resembles an electrical circuit with capacitance and resistance. It breaks down a thermal system into components connected by virtual circuits, with defined interaction properties. The model typically uses air (for the compressor), gas (for the turbine), water (for the bearing housing), and oil (for the bearing housing) as the working fluids. The turbine, compressor, and bearing housing are represented as metal nodes, and the heat storage capacity of these nodes is modeled using capacitors attached to them. The interaction between the nodes is determined using equations for conduction, convection, and radiation. Most common relations to solve for conduction – Newton's law of cooling, for convection - Sieder-Tate correlation or simpler (Dittus-Boelter), for insulated turbocharger studies. Radiation can be neglected; however, Stefan Boltzmann's law could be used to define the radiation effects. Furthermore, experimental measurements may be conducted to determine the parameters needed for solving these thermal processes [13]. Lumped capacitance models in turbochargers assume that work and heat transfer occur separately. The heat transfer is believed to happen before and after the expansion/compression process, while the expansion/compression itself is typically treated as adiabatic. Advantages of the analytical 1-D models are that they are simpler; the lumped capacitance method greatly simplifies the heat transfer equations. It reduces the complex partial differential equations (governing heat conduction and convection) to ordinary differential equations (ODEs), making them much easier to solve; therefore, it is also faster and easier to use compared to 3-D numerical approaches (CHT, CFD…). However, 1-D models need to be validated to establish a reliable foundation. This validation can be achieved through targeted experiments or by using 3-D CHT models. Such validation is crucial for

supporting the results produced by 1-D models. Turbocharger components are typically treated as bodies with well-defined geometries (such as cylinders, discs, and rings). The temperature distribution is assumed to be linear, with radial variations disregarded. 1-D heat transfer models are developed and used alongside experimental performance maps to determine the desired operating point of a turbocharger [13]. For capturing radial heat transfer together with axial, 2-D analytical models have developed, which are still cheaper and easier than experimental methods or 3-D numerical approaches.

1-D and 2-D models are best For, early-stage design and engineering calculations where high precision is not yet critical, the lumped capacitance method provides a quick and cost-effective approximation. Additionally, the method avoids the need to know the complex geometry of the object in detail. Since the lumped capacitance approach assumes a uniform temperature distribution, it doesn't require modeling the geometry or considering temperature variations at different points within the object.

7. Selected software for the analysis (Finite element method).

To analyze rotor temperature field and rotor surface deformation at the location of the journal bearing, a numerical approach was used. The finite element method (FEM) is one of the powerful toolsfor the numerical solution in engineering problems.

7.1. Structural Analysis

The finite element approach is probably used the most frequently in structural analysis. In addition to civil engineering structures like bridges and buildings, the term structural (or structure) also refers to mechanical, aeronautical, and naval structures like aircraft bodies and machine housings, as well as mechanical parts like pistons, tools, and machine parts [15]. Displacements are the main unknowns (nodal degrees of freedom) calculated in structural analysis. The nodal displacements are then used as a starting point to calculate other values, such as strains, stresses, and reaction forces. There are 7 types of structural analysis in ANSYS: static analysis, modal analysis, harmonic analysis, transient dynamic analysis, spectrum analysis, buckling analysis, and explicit dynamic analysis. Between them in this work only static analysis will be present, which is used to determine displacements, stresses, etc. Under static loading conditions, both linear and nonlinear static analysis. Nonlinearities can include plasticity, stress stiffening, large deflection, large strain, hyper elasticity, contact surfaces, and creep [15].

7.2. Definition of Steady-state thermal analysis

In order to determine the temperatures, thermal gradients, heat flow rates, and heat fluxes in an item that are brought on by thermal loads that do not change over time, steady-state thermal analysis is used. Convection, radiation, heat fluxes (heat flow per unit area), heat generation rates (heat flow per unit volume), and constant temperature boundaries are a few examples of such loads. There are two types of steady-state thermal analyses: linear, with constant material characteristics, and nonlinear, with temperature-dependent material properties [16]. Since most materials' thermal characteristics do change with temperature, nonlinear analysis is typically required.

7.3. Coupled -field Analysis

Another method to analyze thermal and structural load on a computational model is to use coupled- field analysis; this analysis can represent thermal effects coupled with other phenomena. Matrix-coupled ANSYS components or sequential load-vector coupling between different simulations of each event can be used in a coupled-field analysis. The same ANSYS Mechanical solver can model thermal-structural coupling. Sequential (1 way) and direct (2 way) coupling are the two methods used for coupled-field analysis [16].

7.4. Sequential Coupled - field Analysis

Solving single-field models in a specific order is necessary for an indirectly coupled analysis. The outcomes of one analysis serve as loads for the analysis that comes next. When there is one-way field interaction, this method of analysis is appropriate. As an illustration, a system's response to one field (for instance, thermal) may have a significant impact on how that system responds to another field (for instance, structural), but not the other way around. This approach typically uses fewer special elements than the direct method and is more effective overall.

The indirect coupled-field analysis is resolved using the sequential method. Note that it involves conducting two single-field analyses sequentially (as opposed to simultaneously), using the output from the first analysis as loads for the second analysis. For instance: Thermal-Structural, however, the structural-to-thermal coupling is negligible (strains are so small that the original thermal solution is unaffected) in contrast to the significant thermal-to-structural coupling that is present in many problems (temperatures cause thermal expansion). Since single-field elements canbe used and no multi-field iteration is necessary, this approach is typically preferable to a direct coupled-field analysis when it is appropriate [17].

8. Finite element model of Turbocharger.

The program ANSYS Workbench was largely used for the rotor surface deformation analysis. Since this program uses the finite element method for such problems, it is necessary to define discretized elements in the model and their mesh quality. Firstly, the turbocharger geometry was divided into the four equal parts as shown in figure 10.

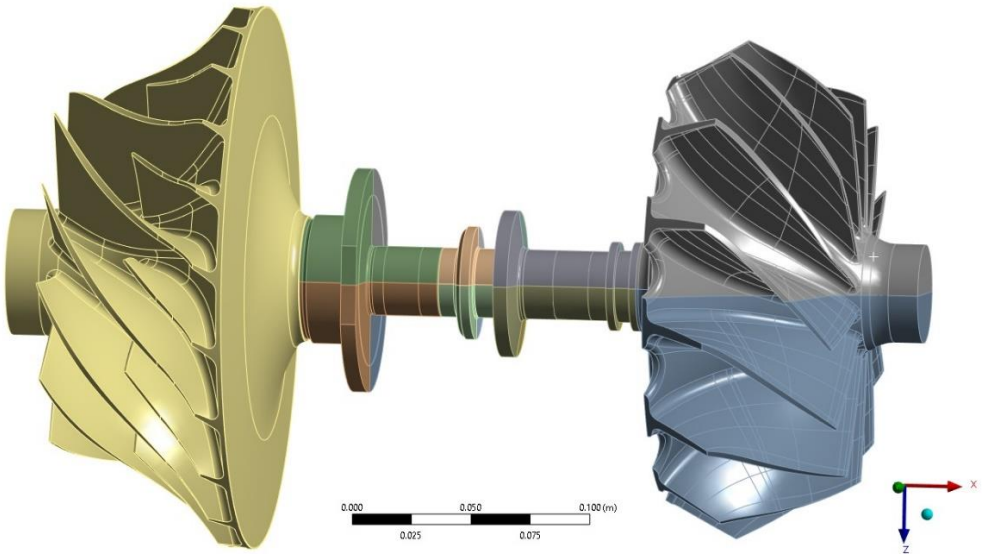

Figure 10. Geometry of the turbocharger model.

For the discretized model, generally, Ansys solid186 elements were used since they are high-order 3D and they have 20 nodes; each of these nodes has 3 degrees of freedom (translation of each node in x, y, and z directions). The element supports plasticity, super-elasticity, creep, stress hardening, large deflection, and large strain capacity. [18] Since it is difficult to create square-shaped elements in problematic areas of the turbocharger geometry, such as blades of turbine andcompressor wheels, tetrahedral, pyramid, and prism methods were introduced. Figure 11 clearly indicates the transition of hexagonal elements into tetrahedral, pyramid, and prism elements.

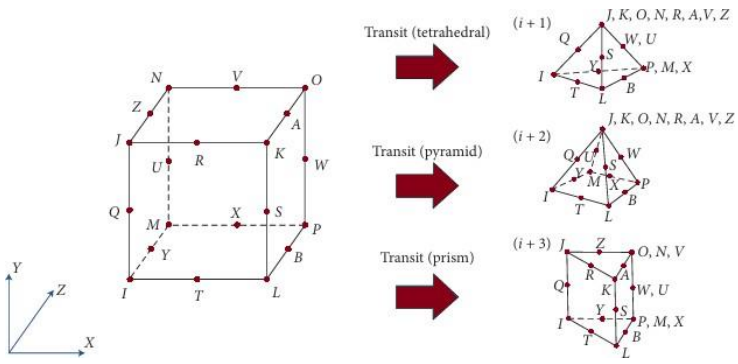

Figure 11. Transition of hexagonal element into, tetrahedral, pyramid and prism elements [18].

After the introduction of geometry, the next step of the FEM analysis was to generate a mesh. For mesh generation, several types of methods have been used for turbine and compressor wheels, since these areas are not the main points of interest and to reduce the number of elements, tetrahedral elements and rough meshing were used; on the other hand, figure 12 and figure 13 illustrate the rotor

bearing system meshed by the hex dominant method, with a much smaller element size compared to turbine and compressor wheels. Also, mesh quality was checked, and from figure 14, it shows that the majority of elements are above 0.5, which is more than enough for the current analysis. In figure 15, the number of nodes and elements is shown, since a lower number of those means less computational time and resources.

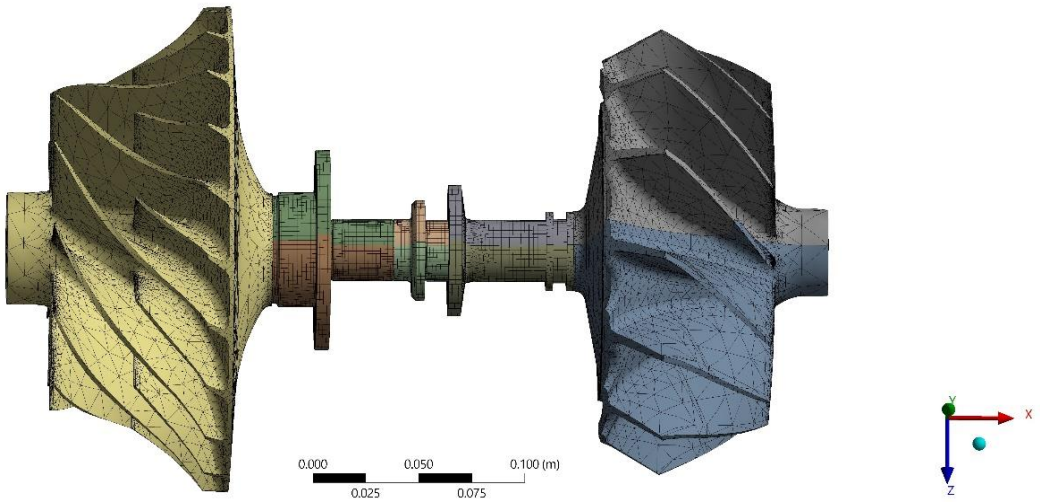

Figure 12. Mesh of the computational model.

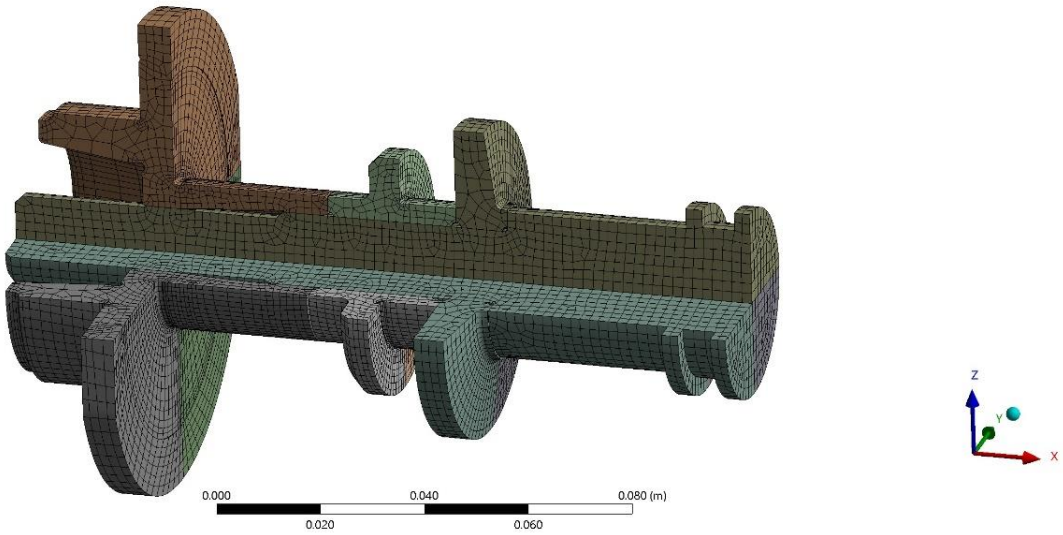

Figure 13. Mesh of the rotor-bearing system.

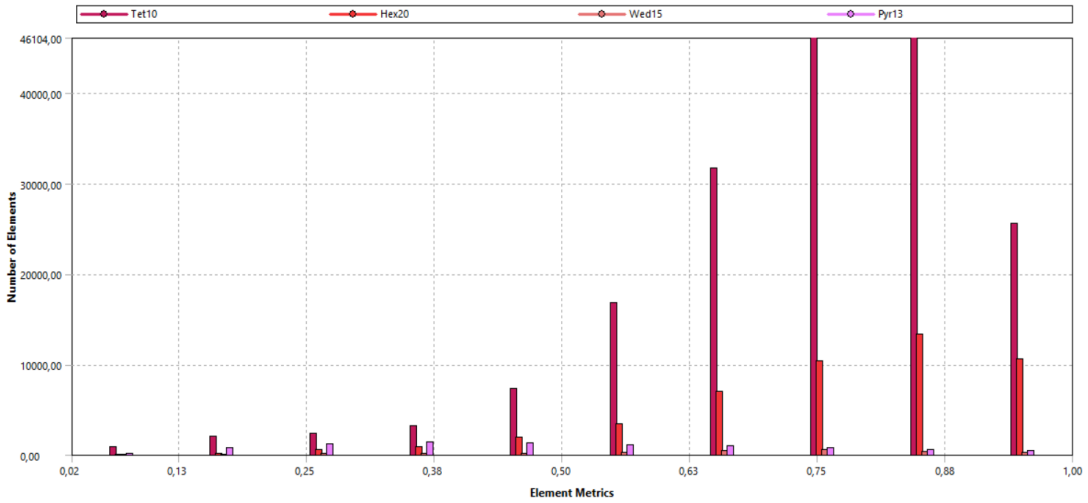

Figure 14. Element quality of mesh.

Quality	
Check Mesh Qua...	Mesh Quality Worksheet
Error Limits	Aggressive Mechanical
Target Elemen...	Default (5,e-002)
Smoothing	Medium
Mesh Metric	Element Quality
Min	2,0304e-002
Max	1,
Average	0,73641
Standard Devi...	0,17298
Inflation	
Advanced	
Statistics	
Nodes	540679
Elements	239796

Figure 15. Number of elements and nodes.

Furthermore, based on [18], to establish the equation of motion for each element, the effects of rotational inertia, translational inertia, gyro moment, support stiffness, support damping, material damping, rotational damping, and thermal stress stiffness were considered in the model. The node displacement vector (q_e) of the i^{th}element is:

$$(17)\ q_e = \{x_{ij},\ y_{ij},\ z_{ij}, \dots, x_{iA},\ y_{iA},\ z_{iA}, \dots, x_{iB},\ y_{iB}, z_{iB} \dots\}^T.$$

Where, I, J, K, L, M, N, O, P, Q, R, S, T, U, V, W, X, Y, Z, A, B are the numbers of node and T superscript is the indicator of transposition for matrix or vector.

If we combine equations and boundary conditions for all the elements, the equation of motion of the rotor-bearing system will take the following form:

$$(18)\ \boldsymbol{M}\, q''(t) + \boldsymbol{C}\, q'(t) + \boldsymbol{K}\, q(t) = f(t).$$

Where, $\boldsymbol{M} = \boldsymbol{M_{trs}} + \boldsymbol{M_{rot}}$; $\boldsymbol{C} = [-\Omega\, \boldsymbol{G} + \boldsymbol{C_{con}} + \boldsymbol{C_{brg}}]$; and $\boldsymbol{K} = [\boldsymbol{K_{brg}} + \boldsymbol{K_{sp}} + \boldsymbol{K_{el}} + \boldsymbol{K_{tem}}]$. In these equations, $\boldsymbol{M}$ is a mass matrix including $\boldsymbol{M_{trs}}$ mass components caused by translation along the axis and $\boldsymbol{M_{rot}}$ caused by rotation along the axis. $\boldsymbol{C}$ represents damping matrix with components $\boldsymbol{G}$ - skew-symmetric gyro matrix, $\boldsymbol{C_{brg}}$ - damping matrix caused by floating ring bearing support, $(\boldsymbol{C_{con}} = a \cdot \boldsymbol{K_{con}})$ - constant structural damping with hysteresis characteristics caused by internal friction of the material [18]; Ω - is the rotor speed in (rpm). a – stiffness damping coefficient $\left(\frac{\mathrm{Ns}}{\mathrm{m}}\right)$ Also known as Rayleigh damping, and finally $\boldsymbol{K}$ is the stiffness matrix $\left(\frac{\mathrm{N}}{\mathrm{m}}\right)$. It consists of $\boldsymbol{K_{brg}}$ a stiffness matrix caused by the floating ring bearing support, a spin-softening matrix $\boldsymbol{K_{sp}}$ generated by rotation of the rotor, $\boldsymbol{K_{el}}$ – elastic modulus stiffness matrix, and $\boldsymbol{K_{tem}}$ is the stiffness matrix caused by nonuniformly distributed thermal stress and deformation due to temperature change [18]. $F(\mathrm{t}), q(\mathrm{t})$ are the global force and displacement vectors in time, respectively. If the total number of nodes became a, the sizes of all matrices will be $3a$ x$3a$ and vectors $q(\mathrm{t})$ and $F(\mathrm{t})$ will be expressed as equations (19, 20).

$$(19)\quad q(\mathrm{t}) = \begin{Bmatrix} [x_1(\mathrm{t})x_2(\mathrm{t})x_3(\mathrm{t}), \dots, x_{\mathrm{a}-1}(\mathrm{t})x_{\mathrm{a}}(\mathrm{t})]^{\mathrm{T}} \\ [y_1(\mathrm{t})y_2(\mathrm{t})y_3(\mathrm{t}), \dots, y_{\mathrm{a}-1}(\mathrm{t})y_{\mathrm{a}}(\mathrm{t})]^{\mathrm{T}} \\ [z_1(\mathrm{t})z_2(\mathrm{t})z_3(\mathrm{t}), \dots, z_{\mathrm{a}-1}(\mathrm{t})z_{\mathrm{a}}(\mathrm{t})]^{\mathrm{T}} \end{Bmatrix},$$

$$(20)\quad F(\mathrm{t}) = \begin{Bmatrix} \left[f_{\mathrm{x}1}(\mathrm{t})f_{\mathrm{x}2}(\mathrm{t})f_{\mathrm{x}3}(\mathrm{t}), \dots, f_{\mathrm{x}(\mathrm{a}-1)}(\mathrm{t})f_{\mathrm{xa}}(\mathrm{t})\right]^{\mathrm{T}} \\ \left[f_{\mathrm{y}1}(\mathrm{t})f_{\mathrm{y}2}(\mathrm{t})f_{\mathrm{y}3}(\mathrm{t}), \dots, f_{\mathrm{y}(\mathrm{a}-1)}(\mathrm{t})f_{\mathrm{ya}}(\mathrm{t})\right]^{\mathrm{T}} \\ \left[f_{\mathrm{z}1}(\mathrm{t})f_{\mathrm{z}2}(\mathrm{t})f_{\mathrm{z}3}(\mathrm{t}), \dots, f_{\mathrm{z}(\mathrm{a}-1)}(\mathrm{t})f_{\mathrm{za}}(\mathrm{t})\right]^{\mathrm{T}} \end{Bmatrix}.$$

9. Preparation of computational model.

First, correctly prepare the computational model in terms of materials before proceeding with the FEM analysis. The turbocharger in this analysis uses different materials according to the components. For the compressor wheel—aluminum alloy (2618, T6), for the turbine wheel—Inconel 713 C, and for the shaft—special structural steel (30CrMoV9V ESU). Those materials have different properties correspondingly, and the properties required for analysis are given in the table below.

Table 1. Material properties at 22℃ [19],[20],[21].

Properties at 22℃	Structural Steel (30CrMoV9V ESU)	Aluminum alloy (2618, T6)	Inconel 713 C	SI Unit
Density ρ	7800	2900	8190	kg/m^3
Coefficient of thermal expansion C_p	$1.3 \cdot 10^{-5}$	$2.2 \cdot 10^{-5}$	$1.23 \cdot 10^{-5}$	1/°K
Thermal Conductivity K	39.8	147	9.954	w/m°K

Since we know that the main load on the turbocharger comes from the temperature and its carrier is the air in the case of the compressor and turbine wheels, and for the shaft there is a special engine oil directly in the place of the bearings, it is necessary to know their properties as well. For air, we have two cases: the first is properties of air at an average of 120℃ on the compressor side and properties of air at an average of 540℃ on the turbine side. Their properties are accordingly given in the table below.

Table 2. Properties of air at compressor and turbine side [22].

Properties of Air at 1 atm	Compressor side	Turbine side	SI unit
Avg. Temperature T	120	540	℃
Kinematic viscosity ν	$2.2522 \cdot 10^{-5}$	$8.54 \cdot 10^{-5}$	m^2/s
Thermal diffusivity a_{th}	$3.565 \cdot 10^{-5}$	$1.21 \cdot 10^{-5}$	m^2/s
Thermal Conductivity K	0.03235	0.057	w/m°K
Prandtl Number Pr	0.707	0.703	–

For Engine oil properties SAE 15W-40 was used.

Table 3. Properties of Engine oil SAE 15W-40 [23].

Properties of SAE 15W-40 Engine Oil (Unused) at 370 °K		SI Unit
Prandtl number	300	–
Thermal Conductivity K	0.137	w/m°K
Thermal diffusivity a_{th}	$0.738 \cdot 10^{-7}$	m^2/s
Kinematic viscosity ν	$2.2 \cdot 10^{-5}$	m^2/s
Density ρ	841.8	kg/m^3

In order for the model to be more accurate, the fluid on the free shaft must be taken into consideration as well. Unfortunately, the essence of the liquid is unknown, although we can assume that this liquid consists of a mixture of oil and air. It is impossible to accurately determine their percentage,but we know that it changes with a change in the number of rotations; the slower the rotational speed,the higher the percentage of oil we have. Since, for the analysis to be simplified, a liquid mixture is assumed to have 50% oil and 50% air in it; therefore, to determine its properties, the sum average of air and oil properties has been chosen. Air properties are taken at 100℃ and oil properties are taken at 96.85℃. Values are given in the table below.

Table 4. Properties of liquid mixture of air and oil at 370°K.

Properties of liquid mixture of air and oil at 370°K		SI Unit
Thermal Conductivity K	0.084	w/m°K
Thermal Diffusivity a_{th}	$1.625 \cdot 10^{-5}$	m^2/s
Kinematic Viscosity ν	$2.25 \cdot 10^{-5}$	m^2/s
Prandtl Number Pr	1.386	–

9.1. Boundary conditions for thermal and structural analysis.

For the thermal analysis, it is necessary to first define what the heat transfer coefficient is for the turbocharger components: the compressor, the turbine, the shaft in the place where the bearings are, and for the free surface of the shaft. For the forced convection general form of the Nusselt number (mentioned above in chapter 4.1), which is significant to calculate the heat transfer coefficient, is:

$$(21)\ Nu = a\, Re^{b} Pr^{c}\ .$$

since There is significant forced convection inside the compressor and turbine housing the spiral is modeled as a straight pipe and the heat transfer coefficient can be calculated from the Nusselt number $\frac{D}{2}$ is chosen for the characteristic length [5].

$$(22)\ \ h_{\text{t,c}} = Nu\frac{2K}{D} = 0.046\frac{K}{D}\, Re^{0.8} Pr^{0.4}\ .$$

In the case of a shaft, the conditions are different, since the fluid moves circularly between the two cylinders; we use the formula proposed by [10].

$$(23)\quad h\frac{D_{\text{e}}}{K} = 0.015 Re^{0.8} Pr^{\frac{1}{3}} \left(1 + 2.3\frac{D_{\text{e}}}{L}\right)\left(\frac{D_2}{D_1}\right)^{0.45}.$$

Where, D_{e} is a gap width of the annuli, $D_1$is an outer diameter of the inner cylinder, and D_2 is an

inner diameter of the outer cylinder.

In the figure 16 below, thermal boundary conditions are shown applied to the computational model accordingly to the heat transfer coefficients calculated from the equations mentioned above. Ambient temperature is considered to be 22 degrees Celsius, and oil temperature is 95 degrees Celsius.

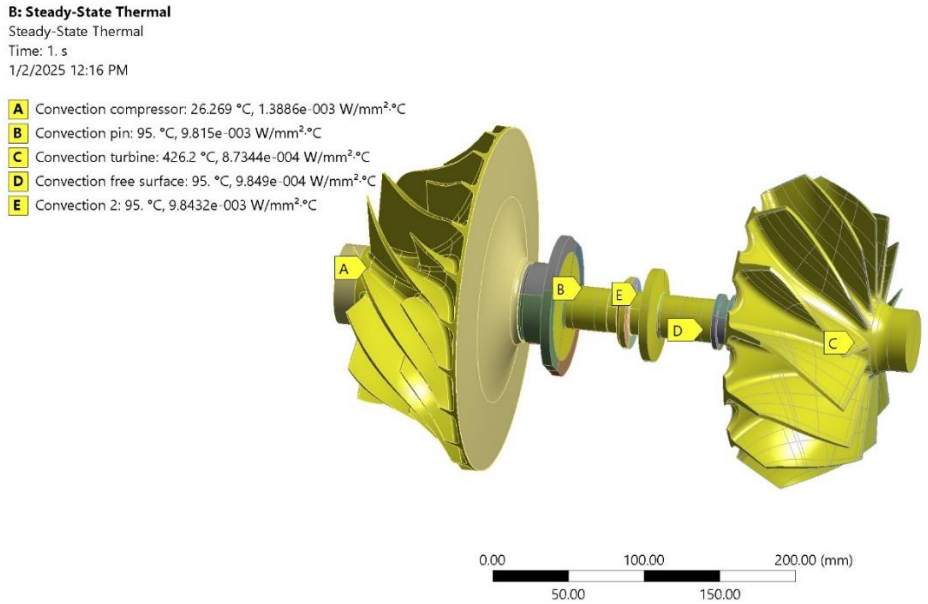

Figure 16. thermal B.C.

Another unknown in the analysis is bolt pretension, but to find it, first bolts must be chosen according to the model of turbocharger. Its dimensions and maximum allowed torque were chosen based on the torque specification table [24]. The model of the turbocharger and permissible torque necessary to fix the turbine, shaft, and compressor were taken from the Garett technical data catalog for different models of turbochargers. The closest option given in the catalog to the model in the analysis is GT40 with minimum and maximum torque on the sides of the compressor and turbine housing, being 20.9 - 24.3 (Nm). The type of bolt is M10 with an allowed range of torque to be 55 ± 10 (Nm). Finally, to find the clamping force on the surface applied by the bolt, the following formula was used:

$$(24)\ t = k\ F_c\ d\ \left(1 - \frac{l}{100}\right)\ .$$

Where t (Nm) is the torque applied on the wrench to tighten the bolts, k is a constant that takes into account bolt material and its size, F_c is the clamping force (N), d is the diameter of the bolt (m), l is the amount of lubrication given, in this case lubrication chose to be with SAE30 oil, presented as a percentage. Note that this formula is an approximation since it does not take into consideration the bolt's thread pitch size.

Except for thermal boundary conditions as a body temperature, a structural analysis set of B.C.s was presented, figure 17 shows bolt pretension calculated from the formula mentioned above, rotational velocity, which represents steady-state conditions, and displacements to avoid rigid body motion. “Remote displacement,” which was used at the ends of turbine and compressor wheels, “displacement” with the X component fixed, and “displacement 2,” which is presented as a line on the shaft with the Y and Z components fixed. After all the boundary conditions were applied, thermo-Structural analysis was carried out.

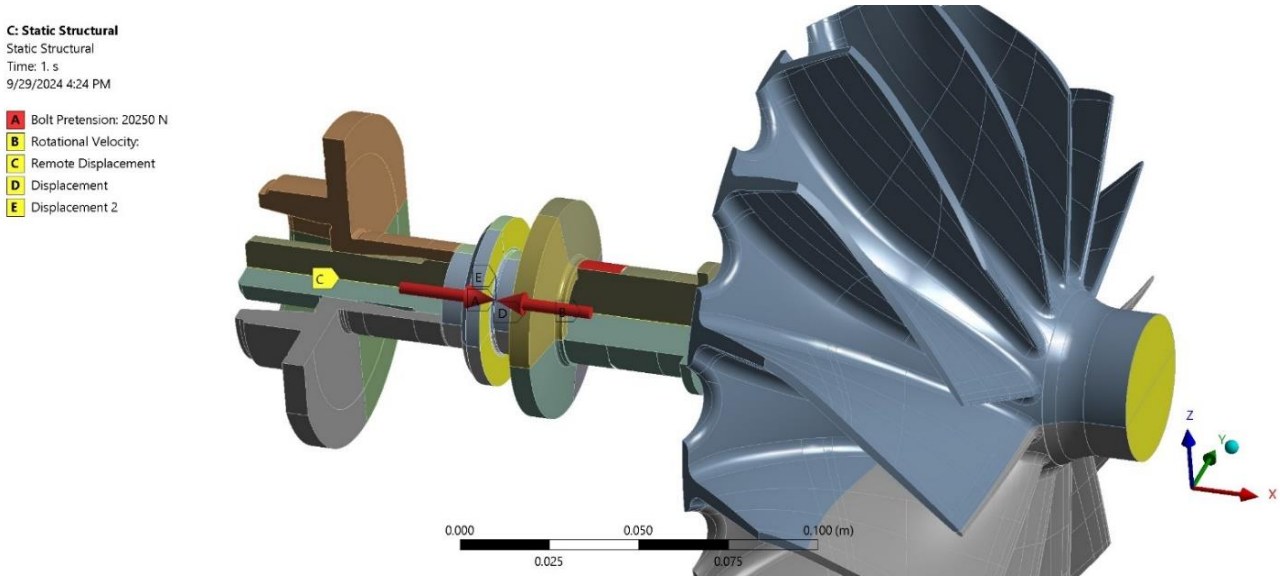

Figure 17. Structural B.C. Section.

10. Results and discussion.

Initially, the analysis of surface deformations of the turbocharger rotor at the location of the radialbearing is performed. For the analysis, ANSYS Workbench was used. Because the acting forces were thermal and structural, coupled analysis was chosen as the type. The known specifications of the turbocharger are given in the table below.

Table 5. Specifications of the turbocharger.

Parameter	value
Outer diameter of Compressor wheel (mm)	175
Outer diameter of Turbine wheel (mm)	170
Diameter of the shaft (mm)	29
Length of the place of radial bearing (mm)	15
Length of the place of thrust bearing (mm)	10.2

Every material with their properties has accordingly been assigned to the parts of the turbocharger. Forthe conservation of computational time and resources, the mesh on the model was refined and used a hexagonal mesh only on the rotor bearing system, turbine wheel, and compressor wheel, which was meshed roughly with tetragons as mentioned above in chapter 8. The technical experiments were carried out at the turbocharger testing facility; the turbocharger was tested in stable operating condition, and as a gas source, a gas burner was used. From this experiment, the gas temperatures for the turbine inlet and outlet - $T_{t,in}$= 659.7 °C, $T_{t,out}$= 424 °C, have been obtained. For compressor inlet and outlet - $T_{c,in}$= 23.8 °C, $T_{c,out}$ = 247.5 °C.

Since the gas temperature is only on the two points (in and out), linear dependence between those points has been assumed. therefore model has defined temperature with the help of linear function; $y = kx + b$. Oil temperature on the rotor bearing system is considered to be 95 $°C$ according to the experimental data. From the thermal analysis, we have got the temperature values on the surface of the turbocharger with the acceptable deviation from the experimental data. Results from thermal analysis are illustrated by the corresponding figures shown below: From only temperature distributions across the shaft at the location of bearings, it is evident that maximum deformation and thus a problematic area will be the radial bearing placed on the turbine side, since maximum temperature was presented in that area compared to the other two. This assumption is further acknowledged by results obtained from the structural analysis, which will be shown further in this chapter.

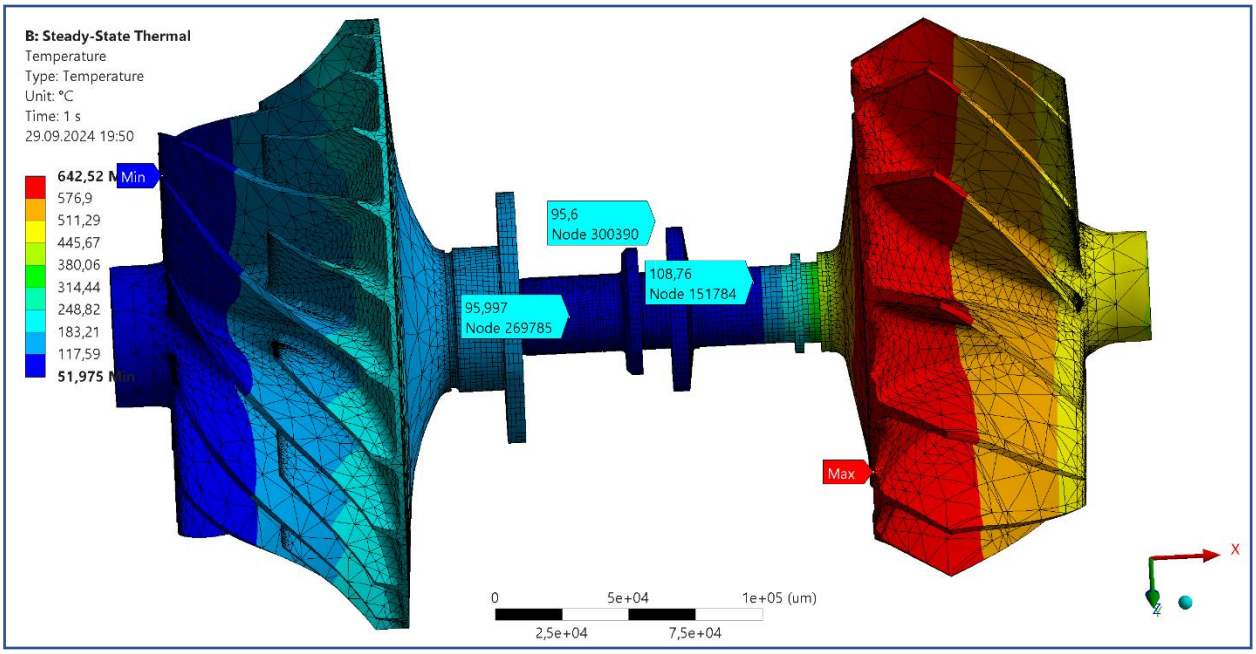

Figure 18. Temperature distribution across the computational model.

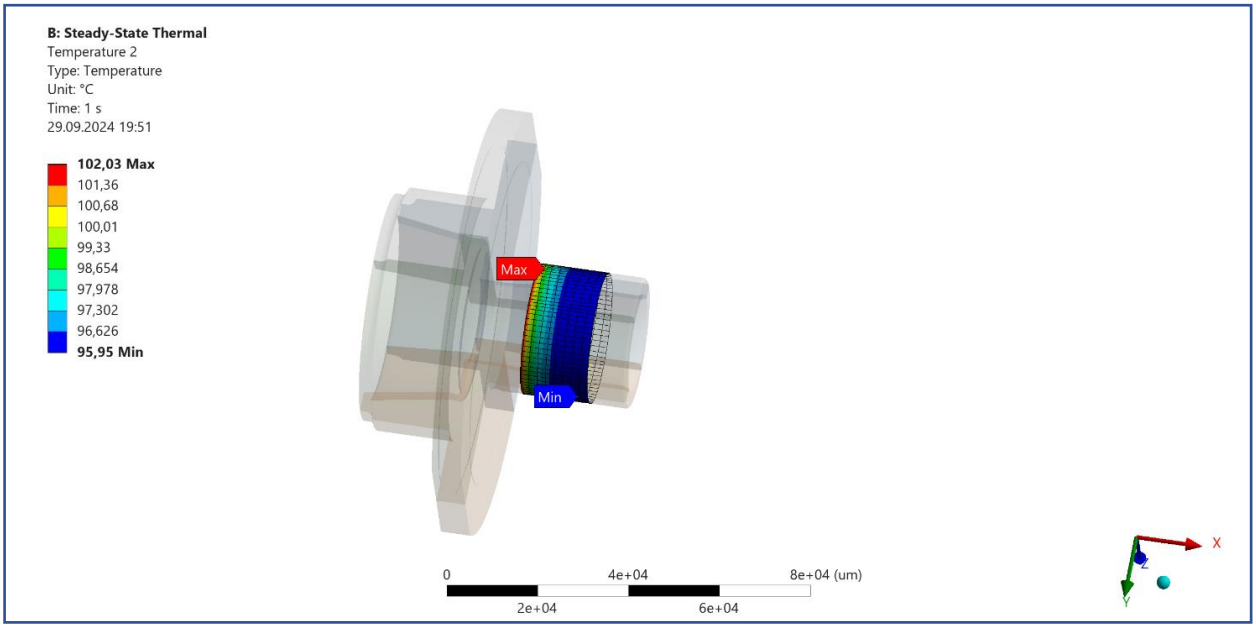

Figure 19. Temperature distribution at the location of radial bearing (**compressor side**).

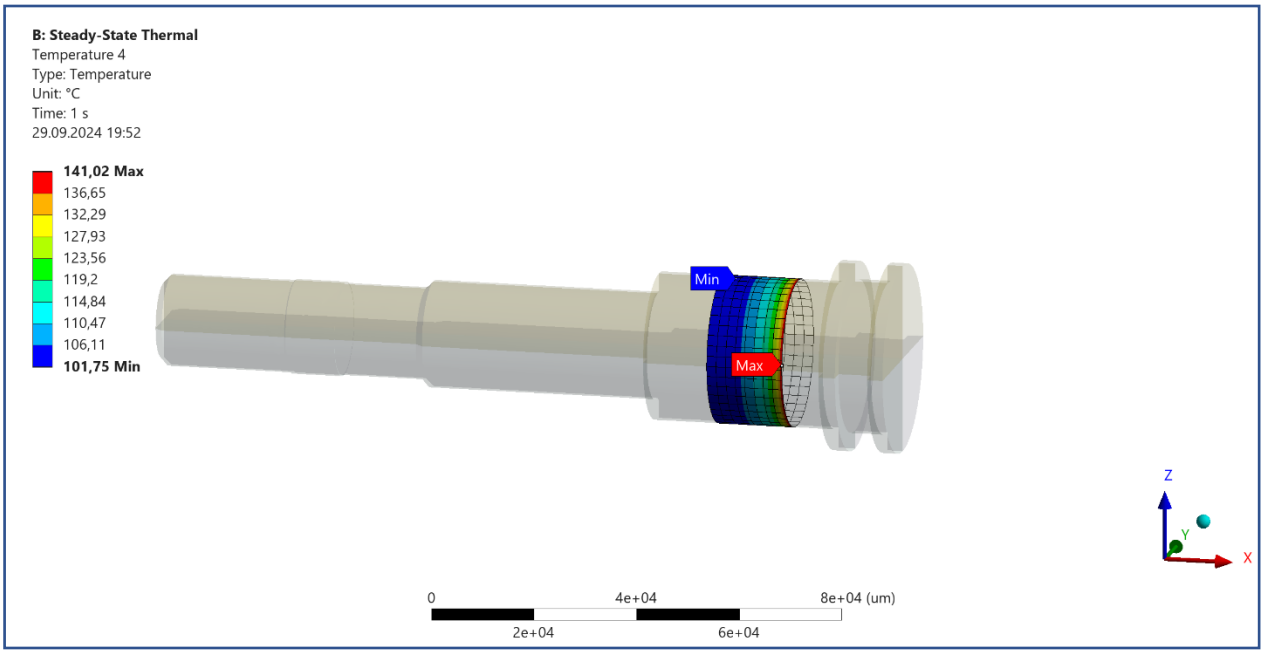

Figure 20. Temperature distribution at the location of radial bearing (**turbine side**).

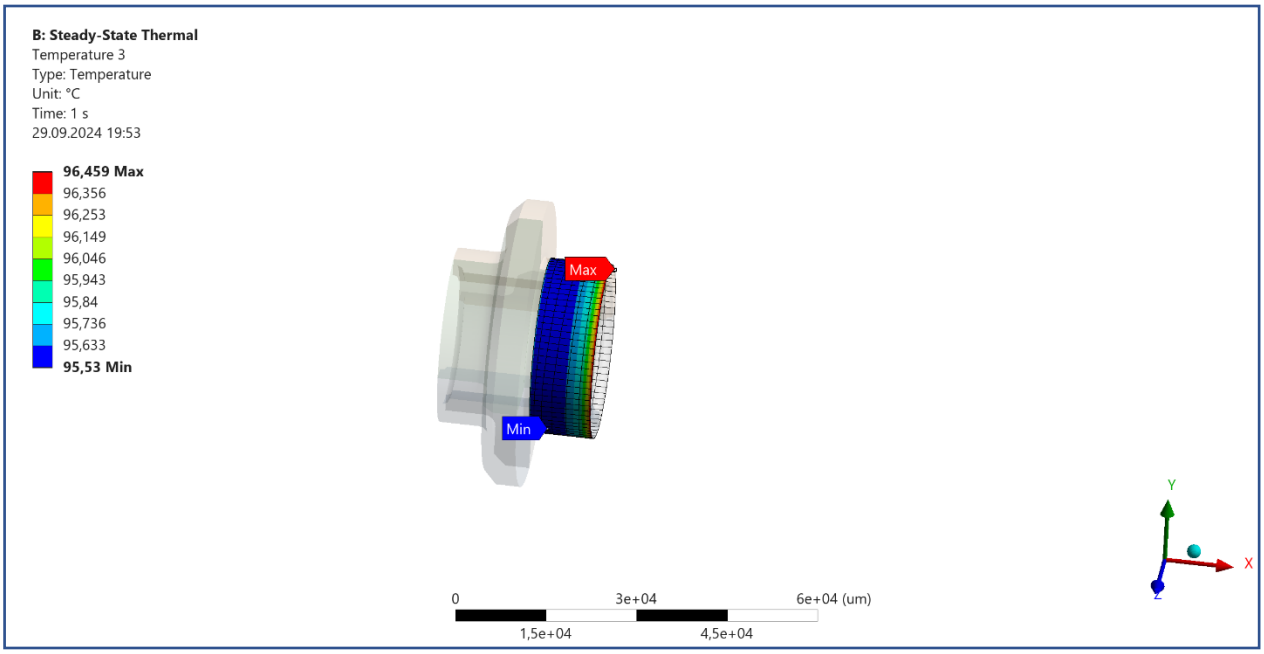

Figure 21. Temperature distribution at the location of **thrust** bearing.

With the help of the results of thermal analysis, a structural analysis was carried out. Analysis divided into three parts, three seconds, each second one load has been added accordingly. Since the first load on the turbocharger came from bolts before the start of operation, 1 second in the analysis only the bolt pretension is present, which will carry on until the end of the analysis. The second step will be the load, which will be applied to the turbocharger during the operation, rotor speed. The

value of the rotor speed has been taken from experimental data as well, which is $N = 47377$ (rpm) or $\left(570\ \frac{\mathrm{m}}{\mathrm{s}}\right)$. The third and final step of the analysis will be the thermal load caused mainly by exhaust gases from turbine operation and pressurized air from compressor operation accordingly. To define the value of bolt pretension, the formula mentioned above was used (24). From this equation, with the maximum allowed torque of TC at the compressor and turbine housing. (24.3 Nm), assuming 40% lubrication with SAE 30 oil and a diameter of the bolt body (10mm), the clamping force is 20250 (N), similarly for defining the values of heat transfer coefficients (22) and (23). Formulas were used. For turbine and compressor values of heat transfer coefficient are given in the table below. Air velocities are calculated from the formula:
$N = \frac{60}{2\pi r} V$. Where, $V\left(\frac{\mathrm{m}}{\mathrm{s}}\right)$ is the velocity and r being the radius, for the compressor wheel it is 0.11421 m. and for turbine 0.1055 m.

Table 6. Heat transfer coefficients and other parameters for compressor and turbine.

Parameter	Compressor	Turbine
Radial Dimension (m)	0.875	0.85
Air velocity $V\left(\frac{\mathrm{m}}{\mathrm{s}}\right)$	566.63	523.41
Reynolds number $Re\ (-)$	4044147.5	1041916.86
Kin. Visc. Of air $\nu_{\mathrm{air}}\left(\frac{\mathrm{m}^2}{\mathrm{s}}\right)$	$2.522 \cdot 10^{-5}$	$8.54 \cdot 10^{-5}$
Prandtl number $Pr\ (-)$	0.7074	0.703
Thermal Conductivity of air $K_{\mathrm{air}}\left(\frac{\mathrm{W}}{\mathrm{m°K}}\right)$	0.03235	0.057
Heat transfer coefficient $h\left(\frac{\mathrm{W}}{\mathrm{m^2°K}}\right)$	1388.64	873.44

Initially, the heat transfer coefficient for the shaft at the location of the radial and thrust bearing and also for the free surface on the shaft is shown accordingly in the table below. In the equation (19) for the calculation of Reynolds number $Re = \frac{(V_{\mathrm{a}} D_{\mathrm{e}})}{\nu}$; mean velocity was used $V_{\mathrm{a}} = \frac{V}{2}$, according to the source provided by [10].

Table 7. Heat transfer coefficients and other parameters for the shaft at the location of radial and thrust bearings.

Parameter	**Location of radial bearing**	**Location of thrust bearing**
Outer diameter of the inner shaft D_1 (m)	0.029	
Diameter of the gap D_e (m)	$4 \cdot 10^{-5}$	
Inner diameter of the outer shaft D_2 (m)	0.02904	
Oil velocity V_{oil} $\left(\frac{m}{s}\right)$	72	
Length L (m)	0.015	0.0102
Reynolds number Re $(-)$	65.45	
Prandtl number Pr $(-)$	300	
Heat transfer coefficient h $\left(\frac{W}{m^2 °K}\right)$	9815	9844

For the "free surface" of the shaft, the same formula was used since the working conditions are similar, but with the assumptions of the length L and gap diameter D_e to be the same, due to lack of information about it. (Theoretically it should be a little bigger than D_e). The heat transfer coefficient for the shaft in the location where there is no bearing is, $h = 984.9$ $\left(\frac{W}{m^2 °K}\right)$.

After knowing all these important parameters, an analysis of the problem was carried out. The surface deformation along with the temperature distribution of the turbocharger rotor at the location of the radial and axial bearings is presented in the following figures.

Results from structural analysis:

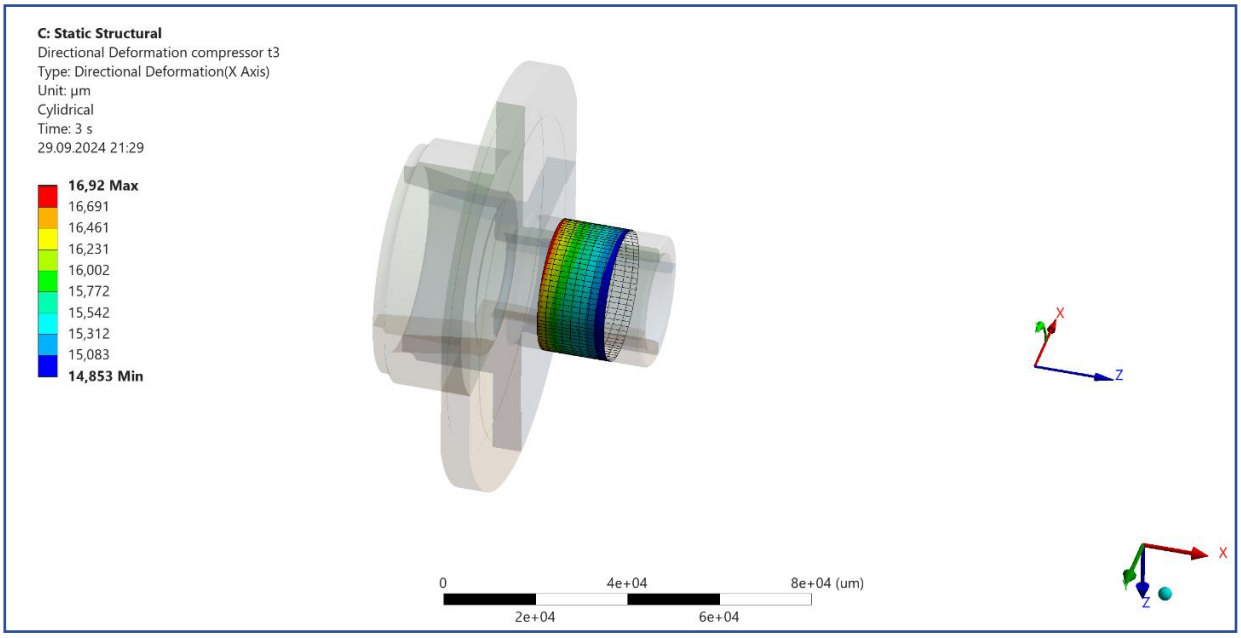

Figure 22. Directional deformation of the shaft at the location of radial bearing (Last timestep, **compressor side**).

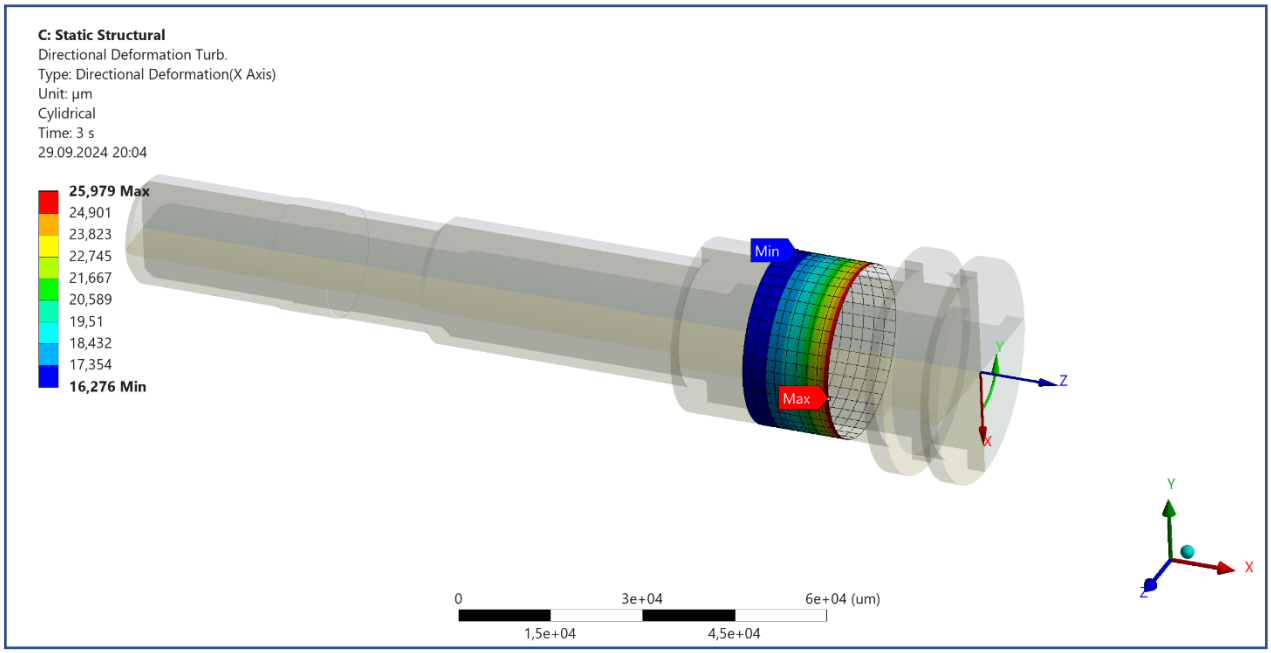

Figure 23. Directional deformation of the shaft at the location of radial bearing (Last timestep, **Turbine side**).

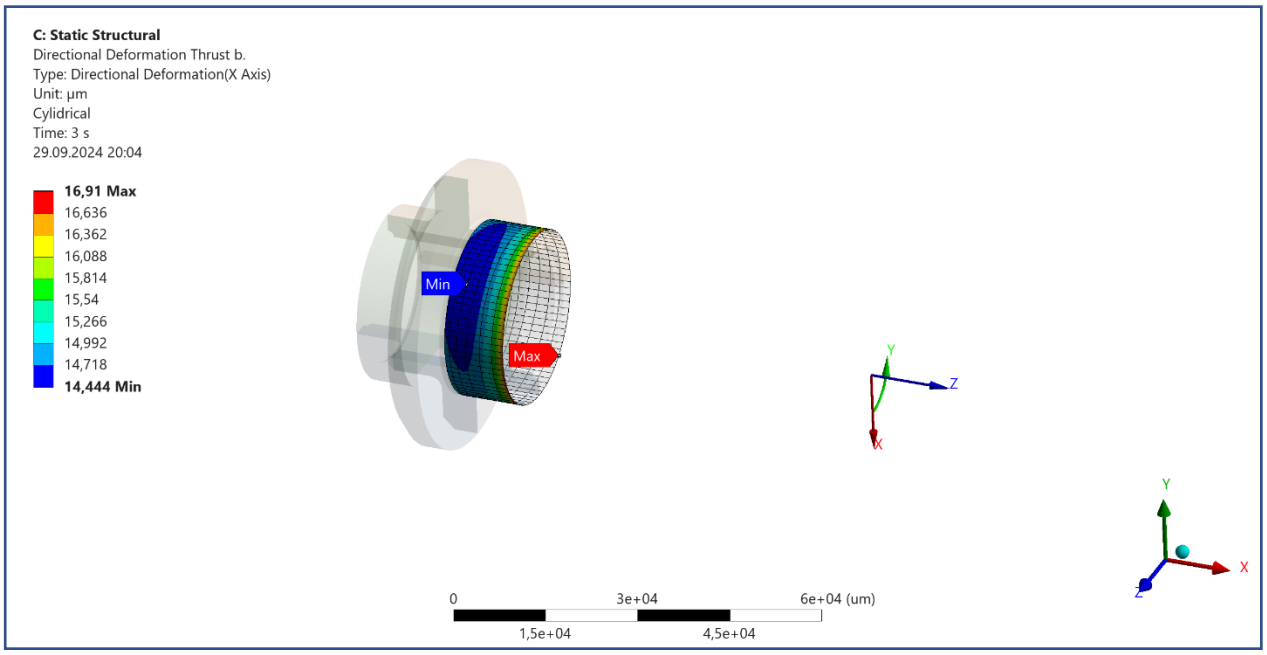

Figure 24. Directional deformation on the shaft at the location of **thrust bearing** (Last timestep).

From the figures mentioned below, since deviations of results on circumference of the shaft, are small (several tenth of micrometers), results can be presented in 2D coordinate system as well.

Deviation of results:

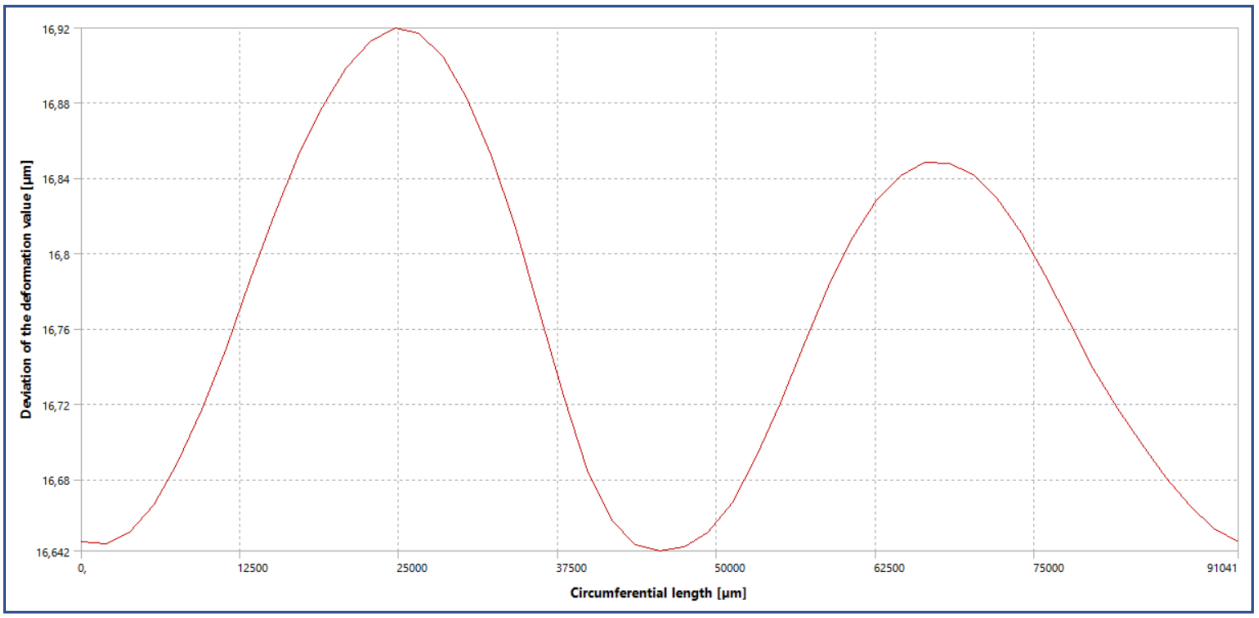

Figure 25. Deviation of result values on circumference of the shaft (**compressor side**).

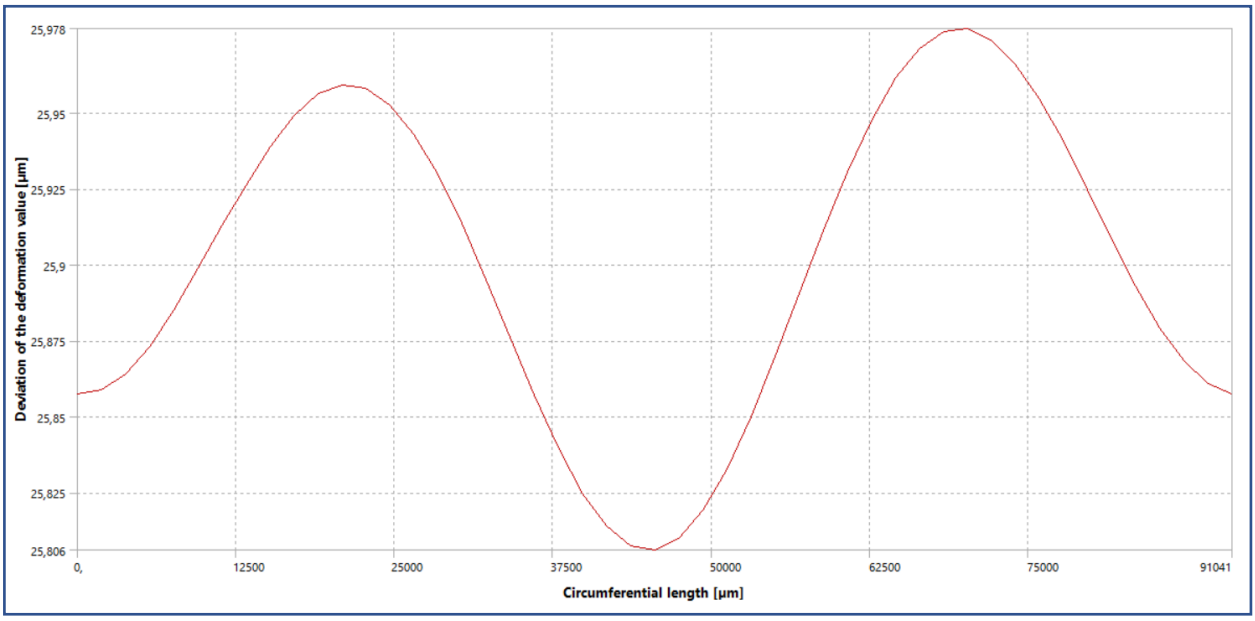

Figure 26. Deviation of result values on circumference of the shaft (**turbine side**).

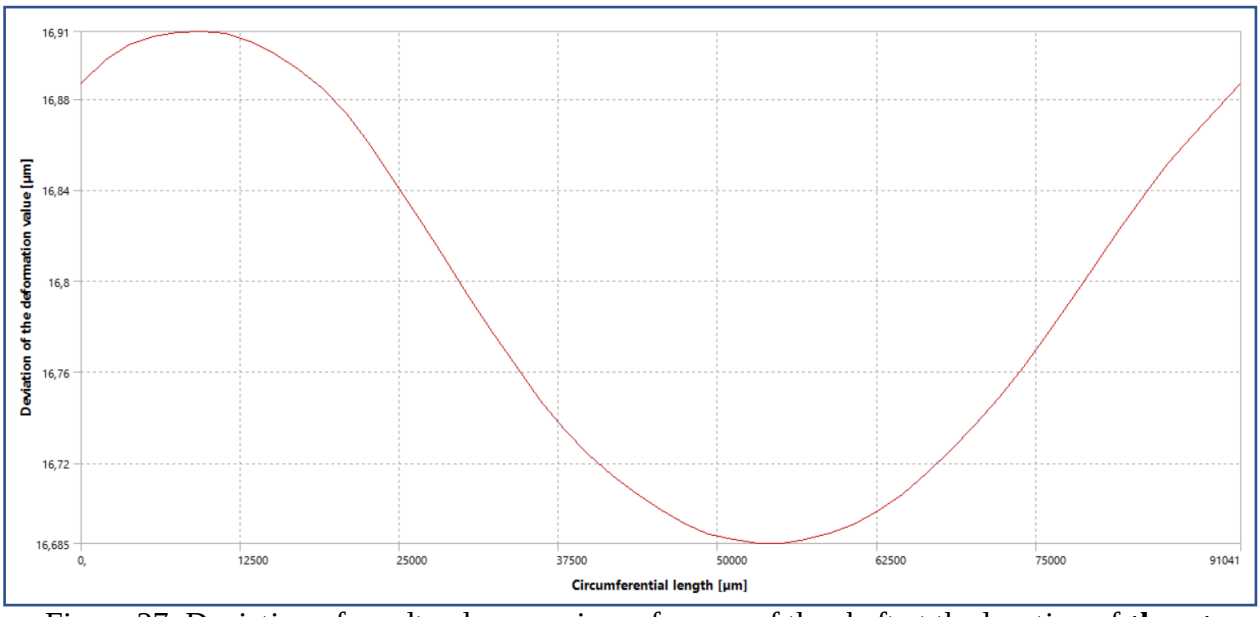

Figure 27. Deviation of result values on circumference of the shaft at the location of **thrust bearing**.

Results from structural analysis in 2D graph (Compressor side):

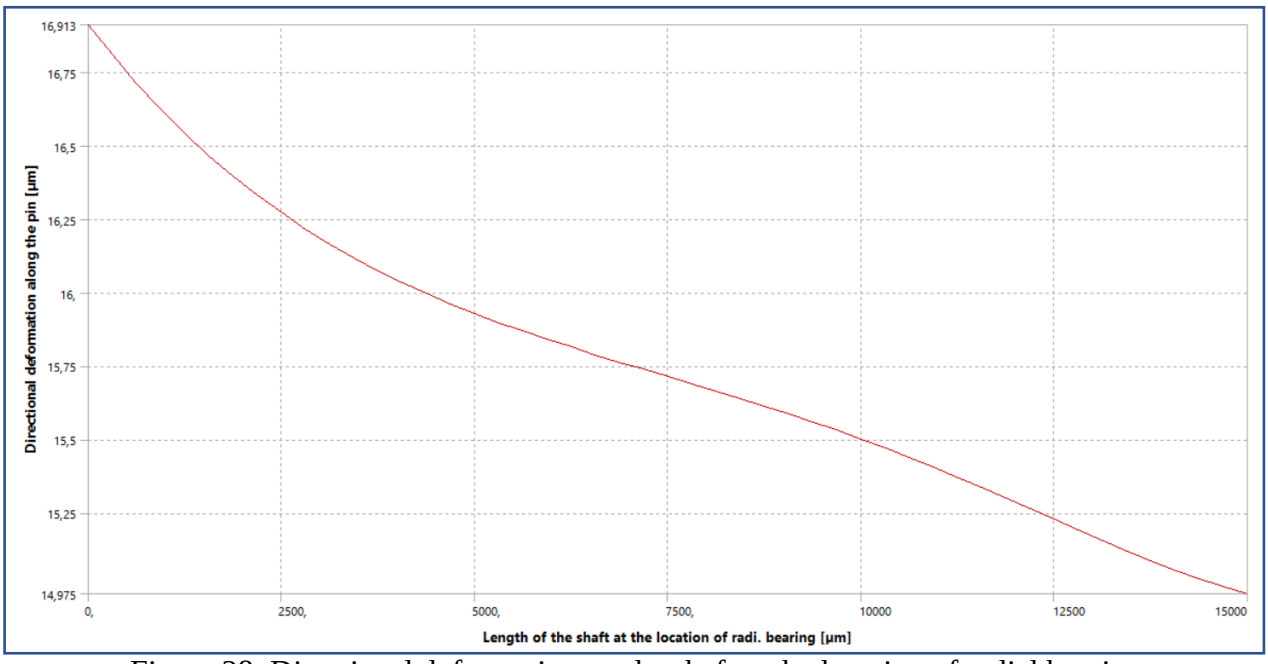

Figure 28. Directional deformation on the shaft at the location of radial bearing (Last timestep **compressor side**).

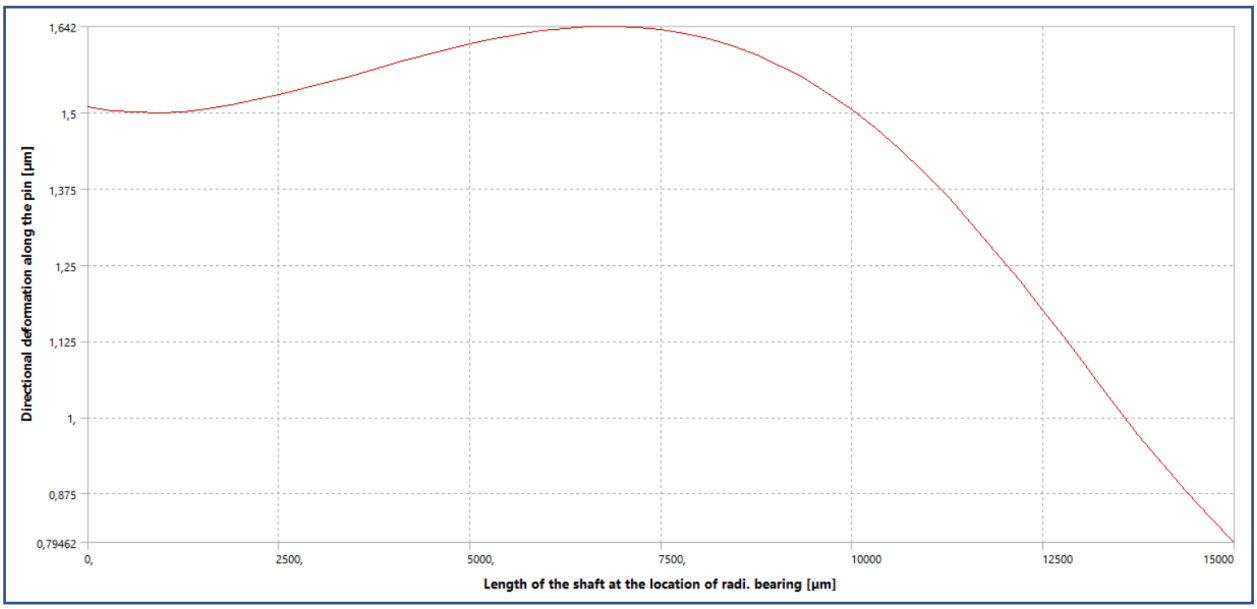

Figure 29. Directional deformation on the shaft at the location of radial bearing (2nd timestep **compressor side**).

Results from structural analysis in 2D graph (Turbine side):

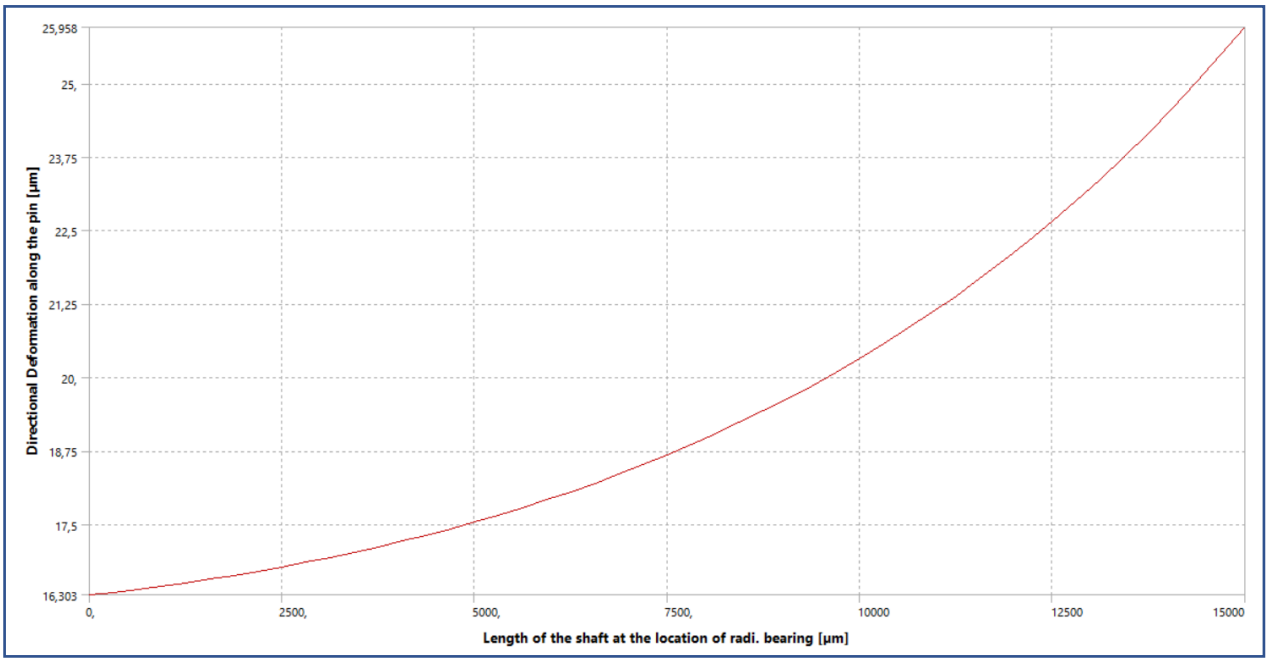

Figure 30. Directional deformation on the shaft at the location of radial bearing (Last timestep **turbine side**).

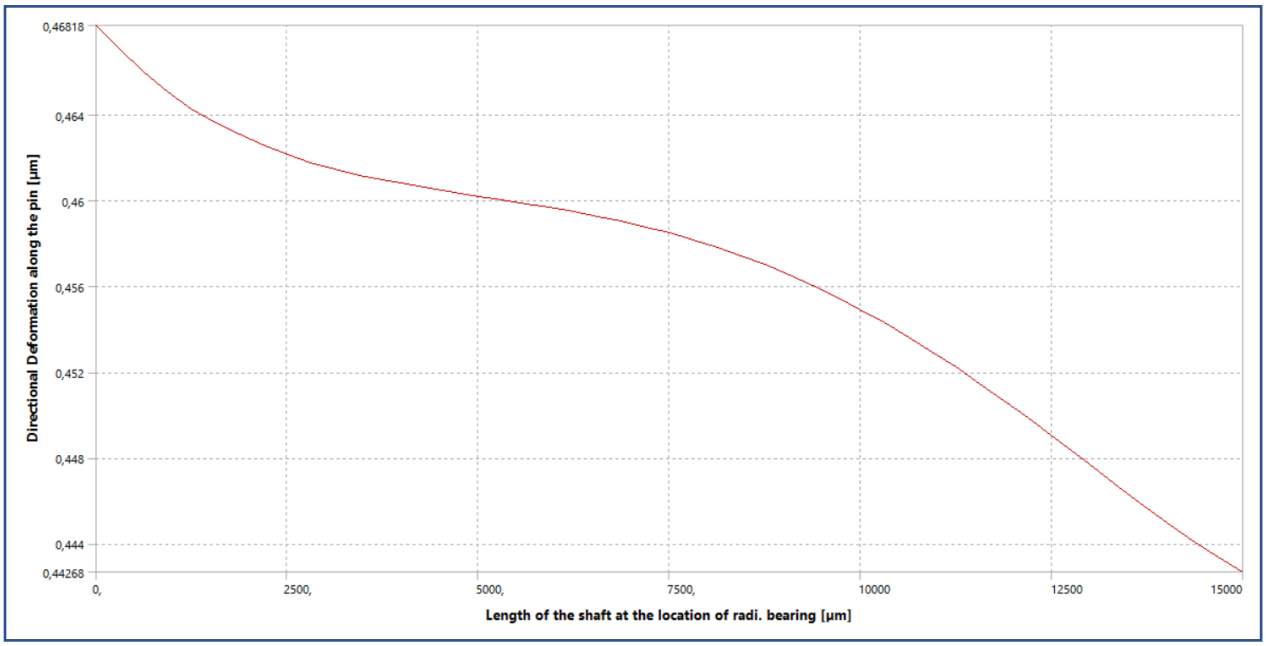

Figure 31. Directional deformation on the shaft at the location of radial bearing (2nd timestep **turbine side**).

Results from structural analysis in 2D graph (Thrust bearing):

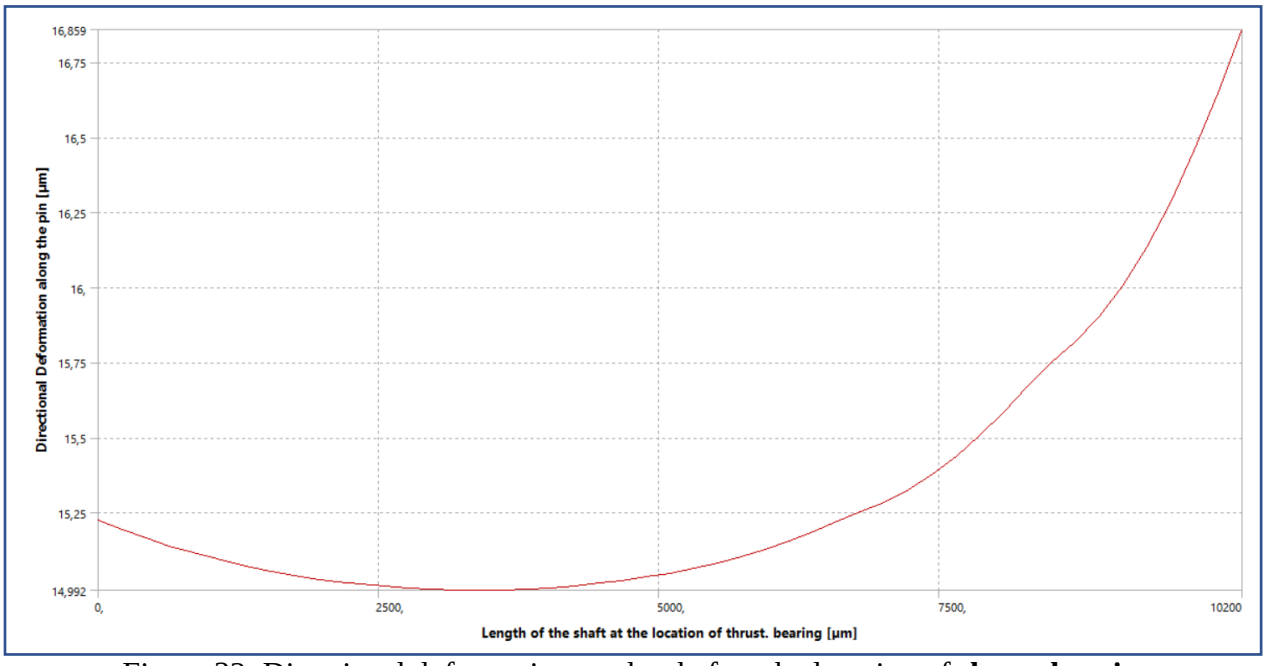

Figure 32. Directional deformation on the shaft at the location of **thrust bearing** (Last timestep).

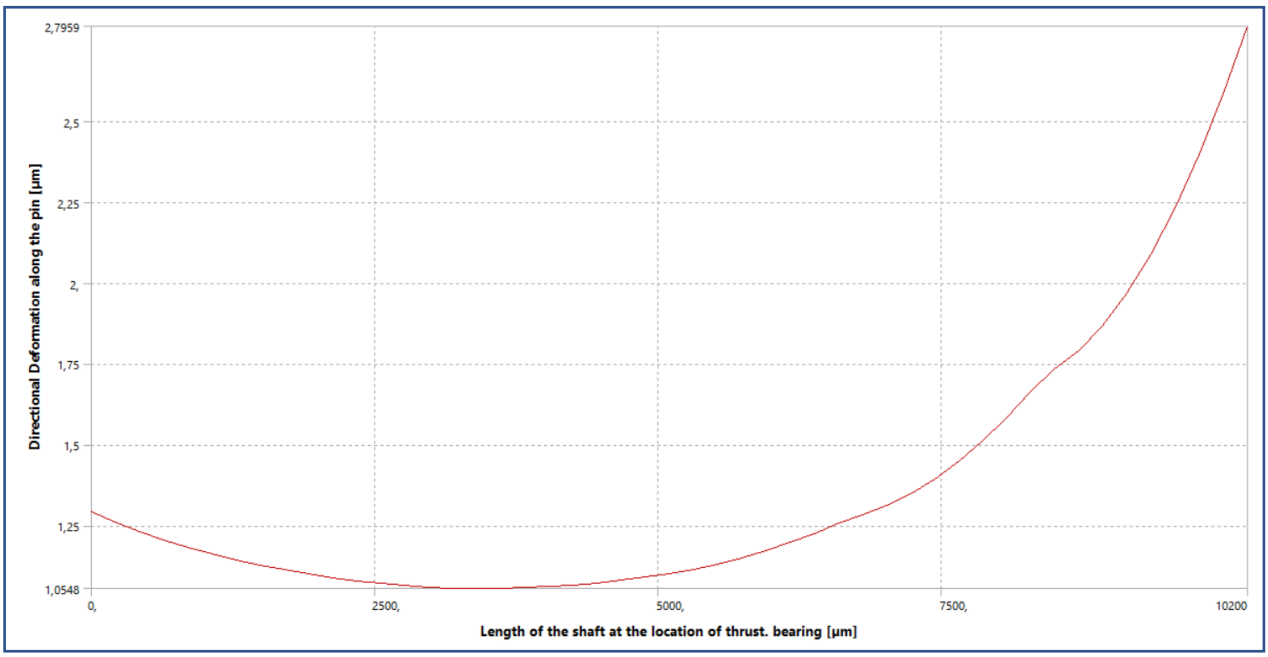

Figure 33. Directional deformation on the shaft at the location of **thrust bearing** (2nd timestep).

First of all, from the circumference figures (25), (26), and (27), it is evident that the maximum deviation of results around the circumference of the rotor is only 0.278 micrometers, which is acceptable. And from the graphs of directional deformation along the shaft at the location of bearings, it is safe to say that the primary source of deformation is definitely caused by the thermal loads because the major deformation increased after the 2nd time step when the thermal load was being introduced. Furthermore, to somewhat verify the results, a simple formula for calculating the change of dimension of the body caused by the temperature increase - $D = D_0(1 + C_p \Delta T)$. where D (m) is the new diameter of the cylinder body after the thermal expansion, D_0 (m) is the initial diameter of the cylindrical body, ΔT is the temperature gradient, ambient temperature is considered to be 21-22 °C, and C_p is the coefficient of thermal expansion $\left(\frac{1}{°K}\right)$. It measures the fractional change in size per degree change in temperature at a constant pressure for the special structural steel (30CrMoV9V ECU) $C_p = 1.3 \cdot 10^{-5} \left(\frac{1}{°K}\right)$. For the maximum deformation of the shaft at the location of the bearing, which is naturally on the turbine side, analytically we get circular

deformation 45.25 (μm). While numerically, deformation is 51.916 (μm). The 12.84% difference between these two results is because the numerical solution only considers linear thermal expansion of the body, whereas the analytical solution includes deformation due to bolt pretension rotation and nonlinear effects.

11. Conclusion.

This research aimed to analyze the surface deformation of the turbocharger rotor at the location of the radial bearing, focusing on both thermal and structural analyses. The results indicate that the primary source of deformation is the thermal load acting on the shaft, which is a critical factor in the design of the rotor's structure. Significant deformation of the pin suggests that further optimization of the rotor-bearing system is necessary.

ANSYS Workbench was used to obtain these results. Initially, a thermal model was developed to approximate the heat transfer process from the compressor and turbine wheels to their connecting pin. The results from the thermal analysis were then applied as a load on the system, in addition to bolt pretension and rotational loads. During the structural analysis, contact interactions between parts of the computational model were examined using the contact tool, with no non-zero pressure at the contact regions, confirming the validity of the results. The last and most important time-step of surface deformation results can be seen in Table 8 at the location of the radial and thrust bearings.

Table 8. surface deformation of the turbocharger rotor at the location of the radial and thrust bearing.

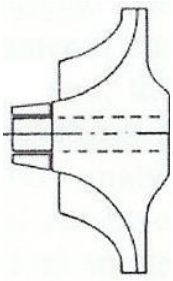

Time-step	Radial bearing (C)		Thrust bearing			Radial bearing (T)		Unit
	Comp. side	Turb. side	Comp. side		Turb. side	Comp. side	Turb. side	
Last	16.91	14.98	15.25	14.99	16.86	16.30	25.95	[μm]

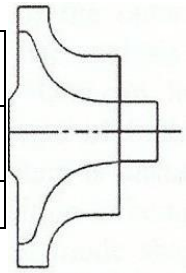

Compressor wheel [25] Turbine wheel [25]

Since the method only uses one software and mesh of the model is optimized, the results can be obtained quickly with acceptable accuracy. This method is efficient and relatively easy to implement compared to more complex techniques, such as conjugate heat transfer (CHT) or computational fluid dynamics (CFD), which may require more specialized user experience. Although, if the working conditions change from steady-state to transient, the analysis process can be time-consuming and complex.

For future research, improvements in the heat transfer modeling could yield more accurate heat transfer coefficients (HTCs). Currently, the compressor and turbine wheels are modeled as cylinders, neglecting their blades, which simplifies the approach but may compromise accuracy. A more detailed modeling of the turbine and compressor volutes could enhance the results' precision. Additionally, since the turbine operates under steady-state conditions and the rotational speed is assumed constant, the results cannot be generalized to applications like automotive turbochargers, where rotor speed fluctuates. Therefore, further research is needed to analyze surface deformation under transient operating conditions.

12. References.

1. Mitchell H. Coupled Field Analysis (with Emphasis on Thermal-Stress) Chapter ppt download [Internet]. Slideplayer.com. 2015 [cited 2024 Jun 17].
2. Stachowiak G, Batchelor AW. Engineering tribology. Butterworth-heinemann; 2013 Sep 16.
3. Hamrock BJ, Schmid SR, Jacobson BO. Fundamentals of fluid film lubrication. CRC press; 2004 Mar 15.
4. Lee GY, Park M, Ahn K. Nonlinear vibration analysis of rotor systems with hydrodynamic journal bearings using harmonic balance method. International Journal of Non-Linear Mechanics. 2025 Mar 1;170:104992.
5. ROMAGNOLI, A. a R. MARTINEZ-BOTAS. Heat Transfer on a Turbocharger Under Constant Load Points. In: Turbo Expo 2009: Power for Land, Sea and Air: Volume 5: Microturbines and Small Turbomachinery; Oil and Gas Applications. ASMEDC, 2009, s. 163-174. ISBN 978-0-7918-4886-9. Dostupné z: doi:10.1115/GT2009-59618.
6. Baines N, Wygant KD, Dris A. The analysis of heat transfer in automotive turbochargers.In: Turbo Expo: Power for Land, Sea, and Air. 2009 Jan 1 (Vol. 48869, pp. 115-126).
7. F. W. Dittus, L. M. K. Boelter, 1930, Publications on Engineering, Vol. 2, pp. 443-461.
8. Gnielinski, V. (1976)**:** *"New equations for heat and mass transfer in turbulent pipe and channel flow"*, International Chemical Engineering, Vol. 16, pp. 359-368.
9. Dixon SL, Hall C. Fluid mechanics and thermodynamics of turbomachinery. Butterworth-Heinemann; 2013 Oct 10.
10. Tachibana F, Fukui S. Convective Heat Transfer of the Rotational and Axial Flow between Two Concentric Cylinders. Bulletin of JSME. 1964;7(26):385–91.
11. Almasi A. Turbo Tips: How to Manage Bolt Connections & Bolt Joints in Turbomachines. Turbomachinery Magazine [Internet]. 2024 Mar 22 [cited 2024 Jun 19];65(1).
12. Łuczyński P, Giesen M, Gier TS, Wirsum M. Uncoupled CFD-FEA methods for the Thermo-structural analysis of turbochargers. International Journal of Turbomachinery, Propulsion and Power. 2019 Nov 28;4(4):39.
13. Lewis MT, Hickey JP. Conjugate Heat Transfer in High-Speed External Flows: A Review. Journal of Thermophysics and Heat Transfer. 2023 Oct;37(4):697-712.
14. Diefenthal M, Łuczyński P, Rakut C, Wirsum M, Heuer T. Thermomechanical

analysis of transient temperatures in a radial turbine wheel. Journal of Turbomachinery. 2017 Sep 1;139(9):091001.

15. RAMAKOTAIAH M, Kumar MS, Babu TR, Teja TR. Stress Analysis on a Turbine Shaft. International Journal of Engineering Research and Technology. 2017;6(8):394-6.
16. Lawrence, Kent L. ANSYS Tutorial: Release 11.0; Structural & Thermal Analysis Usingthe ANSYS Release 11.0 Environment. Ukraine: SDC Publications, 2007.
17. Mitchell H. Coupled Field Analysis (with Emphasis on Thermal-Stress) Chapter ppt download [Internet]. Slideplayer.com. 2015 [cited 2024 Jun 17].
18. Liu Z, Wang R, Cao F, Shi P. Dynamic Behaviour Analysis of Turbocharger Rotor-Shaft System in ThermalEnvironment Based on Finite Element Method. Shock and Vibration. 2020;2020(1):8888504.
19. EN 1.7707 (30CrMoV9) Chromium Steel [Internet]. Makeitfrom.com. [cited 2024 Jun 6].
20. Lumm, James A. Mechanical Properties of 2618 Aluminium Alloy (Final rpt. 1 Oct 65-30 Jun 66); AD-801 499/5/XAB; AFML-TR-66238. United States: Air Force MaterialsLaboratory, 1966.
21. Nickelinstitute.org. [cited 2024 Jun 6]. Available from: https://www.nickelinstitute.org/media/2487/alloys-713c_337.pdf.
22. Edge E, LLC E. Viscosity of air, dynamic and kinematic. Engineers Edge LLC. https://www.engineersedge.com/physics/viscosity_of_air_dynamic_and_kinematic_144. 2018;83.
23. Tarawneh, C. (n.d.). Heat Transfer (p. 19). Available from: HeatTransferBooklet.pdf (utrgv.edu).
24. Senr3130 19 00 - Manuals Service Modules - Specifications | PDF | Screw | Nut (Hardware). Scribd. [cited 2024 Jun 14].
25. Kirk R, Alsaeed A, Gunter E. Stability analysis of a high-speed automotive turbocharger. Tribol Trans. 2007 Jun 26;50:427-34. doi: 10.1080/10402000701476908.

13. List of abbreviation and symbols used.

Symbols	Unit	Name
P	[Pa]	Pressure
q''	$\left[\frac{\mathrm{W}}{\mathrm{m}^2}\right]$	Heat flux
K	$\left[\frac{\mathrm{W}}{\mathrm{m}°\mathrm{K}}\right]$	Thermal conductivity
T	[°C]	Temperature
C_{p}	$\left[\frac{1}{°\mathrm{K}}\right]$	Coefficient of thermal expansion
A	$[\mathrm{m}^2]$	Area
h	$\left[\frac{\mathrm{W}}{\mathrm{m}^2°\mathrm{K}}\right]$	Heat transfer coefficient
E	$\left[\frac{\mathrm{W}}{\mathrm{m}^2}\right]$	Emissivity power
$\boldsymbol{\sigma}$	$\left[\frac{\mathrm{W}}{\mathrm{m}^2°\mathrm{K}^4}\right]$	Stefan-Boltzmann constant $(5.67 \cdot 10^{-8})$
s	$[-]$	Emissivity
G	$\left[\frac{\mathrm{W}}{\mathrm{m}^2}\right]$	Irradiation
a	$[-]$	Absorptivity
ρ	$\left[\frac{\mathrm{Kg}}{\mathrm{m}^3}\right]$	Density
c_{p}	$\left[\frac{\mathrm{J}}{\mathrm{Kg}°\mathrm{K}}\right]$	Specific heat capacity at

		const. pressure
v	$\left[\frac{\mathrm{m}^2}{\mathrm{s}}\right]$	Kinematic viscosity
a_{th}	$\left[\frac{\mathrm{m}^2}{\mathrm{s}}\right]$	Thermal diffusivity
Nu	$[-]$	Nusselt number
Re	$[-]$	Reynolds number
c_{v}	$\left[\frac{\mathrm{J}}{\mathrm{Kg°K}}\right]$	Specific heat capacity at constant volume
S	$\left[\frac{\mathrm{J}}{\mathrm{°K}}\right]$	Entropy
R	$\left[\frac{\mathrm{J}}{\mathrm{mol°K}}\right]$	Universal gas constant (8,314)
V_{vol}	$[\mathrm{m}^3]$	volume
$\boldsymbol{h}$	$\left[\frac{\mathrm{J}}{\mathrm{°K}}\right]$	enthalpy
η	$[-]$	Turbocharger efficiency
Pr	$[-]$	Prandtl number
V	$\left[\frac{\mathrm{m}}{\mathrm{s}}\right]$	Velocity
t	[Nm]	Torque
k	$[-]$	Material constant
F	[N]	Force
$\boldsymbol{M}$	[Kg]	Mass matrix
$\boldsymbol{K}$	$\left[\frac{\mathrm{N}}{\mathrm{m}}\right]$	Stiffness matrix
$\boldsymbol{C}$	$\left[\frac{\mathrm{Ns}}{\mathrm{m}}\right]$	Damping
$F(\mathrm{t})$	[N]	Force vector in time

$q(\mathrm{t})$	[m]	Displacement vector in time
N	[RPM]	Rotor speed
r	[m]	radius

Indexes	
atm	Atmospheric
s	Surface
c	clamp
∞	Ambient
abs	Absorb
sur	Surrounding surface
rad	Radiation
t,c	Turbine and compressor
t,in	Turbine inlet
t,out	Turbine outlet
is	Isentropic
act	Actual
adi.c	Adiabatic, compressor
adi.t	Adiabatic, turbine
diab.c	Diabatic, compressor
diab.t	Diabatic, turbine
adi.is	Adiabatic, isentropic
c,in	Compressor inlet
c,out	Compressor outlet
trs	Translation
rot	Rotation
con	Constant
brg	Bearing

sp	Spin Softening
el	Elastic modulus
tem	Nonuniformly distributed thermal stress
vol	Volume
e	Gap

Abbreviations	
TC	Turbocharger
CAD	Computer-assisted design
FEM	Finite element method
FEA	Finite element analysis
CFD	Computational fluid dynamics
TW	Turbine wheel
TH	Turbine housing
OP1	Operation point 1
OP2	Operation point 2
CHT	Conjugated heat transfer
BT	Bulk temperature
AAY	Analytic adiabatic Y-plus
DYF	Diabatic Y-plus field
TIC	Temperature influence coefficient
TFEA-EXPO	Tensor-flow element-wise adaptive-EXPO
HTC	Heat transfer coefficient
ODEs	Ordinary differential equations
1-D	One-dimensional
2-D	Two-dimensional